

THE PENNSYLVANIA STATE UNIVERSITY
SCHREYER HONORS COLLEGE

DEPARTMENT OF BIOCHEMISTRY AND MOLECULAR BIOLOGY

IDENTIFYING A POTENTIAL DRUG-DRUG INTERACTION BETWEEN TWO ANTIMALARIALS
AND UNDERSTANDING THE INFLUENCE OF LIPID SUPPLEMENT COMPOSITION ON
PLASMODIUM FALCIPARUM

CUYLER H. LUCK
SPRING 2020

A thesis
submitted in partial fulfillment
of the requirements
for a baccalaureate degree
in Microbiology
with honors in Microbiology

Reviewed and approved* by the following:

Manuel Llinás
Professor of Biochemistry and Molecular Biology
Professor of Chemistry
Thesis Supervisor

Ming Tien
Professor of Biochemistry and Molecular Biology
Honors Adviser

* Electronic approvals are on file.

ABSTRACT

Malaria remains a deadly and devastating disease across the globe, with *Plasmodium falciparum* responsible for the majority of cases and deaths. While antimalarials are currently still generally effective, resistance has arisen to all current classes of antimalarials and will spread in the future. To delay resistance in future treatments, combination therapies composed of synergistic drugs targeting different aspects of the parasite's metabolism are desirable, while antagonistic combinations should be avoided. Here I tested for drug-drug interactions between (+)-SJ733 and P218, two candidate antimalarials, using a SYBR Green based fixed-ratio assay. The two drugs appear to act antagonistically, suggesting that they likely would not be an effective combination therapy despite presumably acting on different metabolic pathways. However, this should be confirmed with more optimal plate designs and curve fits as well as with comparisons to known pairs of antagonistic/synergistic antimalarials.

Also explored is the impact that different lipid supplements have on *P. falciparum in vitro*. Human serum is often used as a lipid supplement for *in vitro* culture but is costly and variable between individuals, and different batches generate parasites which are differentially able to transmit to mosquitoes. Albumax, an artificial supplement, is standardized and cheaper, but cannot generate any transmissible gametocytes. Furthermore, several phenotypic changes *in vitro* have been shown in asexual parasites that are cultured in serum, Albumax, or a combination thereof. Metabolomics is being used to understand what metabolic differences exist between those supplements able to generate transmissible gametocytes and those that are not, and between parasites grown in Albumax versus serum.

TABLE OF CONTENTS

LIST OF FIGURES	iii
LIST OF TABLES	iv
ACKNOWLEDGEMENTS.....	v
Chapter 1 An Introduction to Malaria.....	1
Disease Characteristics.....	1
Parasite Properties.....	3
Chapter 2 Investigating Interactions Between SJ733 and P218	6
Background	6
Materials and Methods.....	14
Results.....	21
Discussion	30
Future Directions	33
Chapter 3 Discerning Metabolic Differences in <i>P. falciparum</i> Lipid Supplements	35
Introduction	35
Ongoing Efforts	37
Future Experimental Design.....	39
Appendix A Commonly Used <i>P. falciparum</i> Culturing Protocols	44
Culture Maintenance	44
Washing Blood	44
Sorbitol Synchronization.....	44
Culture Freezing	45
Culture Thawing.....	45
Appendix B Complete Normalized IC ₅₀ Figures for Isobologram Construction	47
BIBLIOGRAPHY.....	51

LIST OF FIGURES

Figure 1: Life cycle of <i>P. falciparum</i>.	4
Figure 2: MMV Supported Projects	7
Figure 3: Prior Metabolomic Fingerprint Analysis of SJ733 and P218 by the Llinás Lab	12
Figure 4: 96 Well Plate Layout for the Determination of the IC₅₀ of P218.	17
Figure 5: 96 Well Plate Layout for the Determination of the IC₅₀ of SJ733	18
Figure 6: 96 Well Plate Layouts for the Investigation of Interactions Between P218 and SJ733	19
Figure 7: IC₅₀ Determination of P218	21
Figure 8: IC₅₀ Determination of SJ733	22
Figure 9: Isobologram Analysis of First Set of SJ733 – P218 Combination Plates	23
Figure 10: Isobologram Analysis of Second Set of SJ733 – P218 Combination Plates	24
Figure 11: Isobologram Analysis of Third Set of SJ733 – P218 Combination Plates	25
Figure 12: Combined Isobologram Analyses of SJ733 – P218 Combination Plates	26
Figure 13: Good vs. Bad Serum Separation from One Sample Set.	38
Figure 14: Sample AlbuMAX to Serum Transition Experiment Layouts	41
Figure 15: Normalized Relative Growth Data for SJ733 from Plate Set 1	47
Figure 16: Normalized Relative Growth Data for P218 from Plate Set 1	48
Figure 17: Normalized Relative Growth Data for SJ733 from Plate Set 2	48
Figure 18: Normalized Relative Growth Data for P218 from Plate Set 2.	49
Figure 19: Normalized Relative Growth Data for SJ733 from Plate Set 3	49
Figure 20: Normalized Relative Growth Data for P218 from Plate Set 3	50

LIST OF TABLES

Table 1: Concentrations of SJ733 and P218 in Solutions 1 Through 6.....	20
Table 2: IC50 Values For Individual Drugs and Combination Replicates	27
Table 3: Derived FIC50 Values.....	28
Table 4: Mean FIC50 Values	29

ACKNOWLEDGEMENTS

Many thanks to my five parents and brother for helping me grow as a person throughout the past 22 years. In the lab, Manuel and the entire group have been instrumental in guiding my development as a scientist, particularly Dr. Erik Allman, Dr. Heather Painter, Dr. Gabe Rangel, Justin Munro, and Ed Owen. Outside of Penn State, the time I spent with Dr. Blaine Bartholomew and his lab at MD Anderson gave me a chance to experiment in a new field and get a taste of full-time research. The two summers I spent in the lab of Dr. Lewis Chodosh at the University of Pennsylvania got me hooked on cancer biology and confirmed my interest in pursuing a PhD after graduation. It has been the combined support of all of these individuals, whether through home-cooked meals, long hours in the lab, or countless recommendation letters, that has guided me to where I am today, and I am truly thankful for their help. Additional thanks to the Eberly College of Science at Penn State for contributing financial support for my research, and to the Millennium Scholars Program and Schreyer Honors College for invaluable mentoring and support over the past four years.

Chapter 1

An Introduction to Malaria

Disease Characteristics

Malaria remains a dangerous and deadly disease with 228 million estimated cases and 405,000 estimated deaths worldwide in 2018¹. The vast majority of these cases occur in India or African countries, and children under the age of 5 bear the brunt of deaths, making up roughly two-thirds of estimated deaths in 2018¹. Pregnant women comprise another uniquely susceptible population (for more information, see the review here²), which together with its impact on children truly makes malaria a disease of the vulnerable. Malaria is largely caused by two species of *Plasmodium* parasite: *P. falciparum* dominates in most affected regions (Africa, South-East Asia, the Eastern Mediterranean, and the Western Pacific) while *P. vivax* plays an important role in the Americas, while also being present in South-East Asia¹. While other *Plasmodium* species can cause malaria in humans and other species of animals, *P. vivax* and *P. falciparum* represent the vast majority of cases in humans and *P. falciparum* is the deadliest parasite that infects humans. It appears that individuals can acquire immunity to the disease, as the severity of the disease tends to decline with age in endemic populations³.

The main symptom of malaria is fever, though additional common ones include headache and nausea among others^{3,4}. It is thought that the immune system's cytokine response to parasite material released during red blood cell lysis in the asexual blood lifecycle may contribute to systemic symptoms of the disease^{3,4}. When treatment does not completely clear the causative parasite, severe malaria can develop, most often in children. Severe malaria mainly presents through three routes: cerebral malaria, metabolic acidosis (usually as respiratory distress), and severe anemia^{3,5}. Contributing to the first two of these is the tendency of *P. falciparum* to obstruct the microvasculature via extracellular proteins which

allow binding to the endothelium and other erythrocytes^{3,5}. Cerebral malaria develops when such obstruction impairs blood flow to the brain and can lead to altered mental state⁴. It can also be defined clinically as parasite-induced coma³. Metabolic acidosis generally arises as cells are forced to turn to the anaerobic generation of lactic acid from glucose⁶, given the decreased oxygen supply due to obstruction of the microvasculature. Anemia is a consequence of the erythrocyte lysis that is part of the asexual blood stage lifecycle, but uninfected red blood cells can be eliminated and contribute to this disorder as well^{3,4}. It has also been noted that this additional loss of erythrocytes may exacerbate existing, chronic anemia³.

Antimalarial drugs have been identified and used for over 100 years, with some of the original compounds retaining efficacy today. A review of some of the key drugs in the history of malaria can be found here⁷. The World Health Organization currently recommends 14 drugs for curative treatment of malaria, and many are either combinations or single drugs to be used in combination with other compounds⁸. Some monotherapies are recommended, but for specific scenarios (e.g. artemether as an oily injection for managing severe malaria). The frontline antimalarials are largely centered upon artemisinin and its derivatives. Combination therapies are emphasized by the WHO because resistance has arisen to all classes of antimalarials, including the artemesinins^{9,10}. While treatments are still efficacious for now, there is a dire need for novel antimalarial drugs as we engage in an arms race with *Plasmodium* parasites.

Parasite Properties

Focusing on *P. falciparum*, the biology of the parasite is complex. The parasite has a lifecycle spread across three main host environments: the human liver, human red blood cells, and the *Anopheles* mosquito. Mosquito bites pass sporozoites into a new human host, which take up residence in the liver. Following multiplication and differentiation into merozoites (the process takes approximately 6.5-7 days^{11,12}), the parasite then enters the blood and undergoes a 48-hour asexual replicative lifecycle where each cycle ends with lysing of blood cells to allow reinfection (see here³ for more information on the liver stage and transmission to erythrocytes). It is this timed cell lysis that gives rise to the disease's classical cyclical fever⁴. Some parasites in this asexual lifecycle will turn into sexual gametocytes (this process takes 10-12 days¹³) for uptake by a new mosquito vector (for a full review on regulation of gametocytogenesis, see here¹³), where the parasites differentiate through multiple steps into sporozoites and begin the lifecycle anew (*Plasmodium* development in the mosquito takes approximately 2 to 3 weeks⁴). For more information on the lifecycle as well as a discussion of various bioluminescent parasites that have been generated for studying different stages of the lifecycle, see here^{4,14}. See the following figure published by J. Alexandra Rowe and colleagues at the University of Edinburgh for a visual representation of the lifecycle¹⁵.

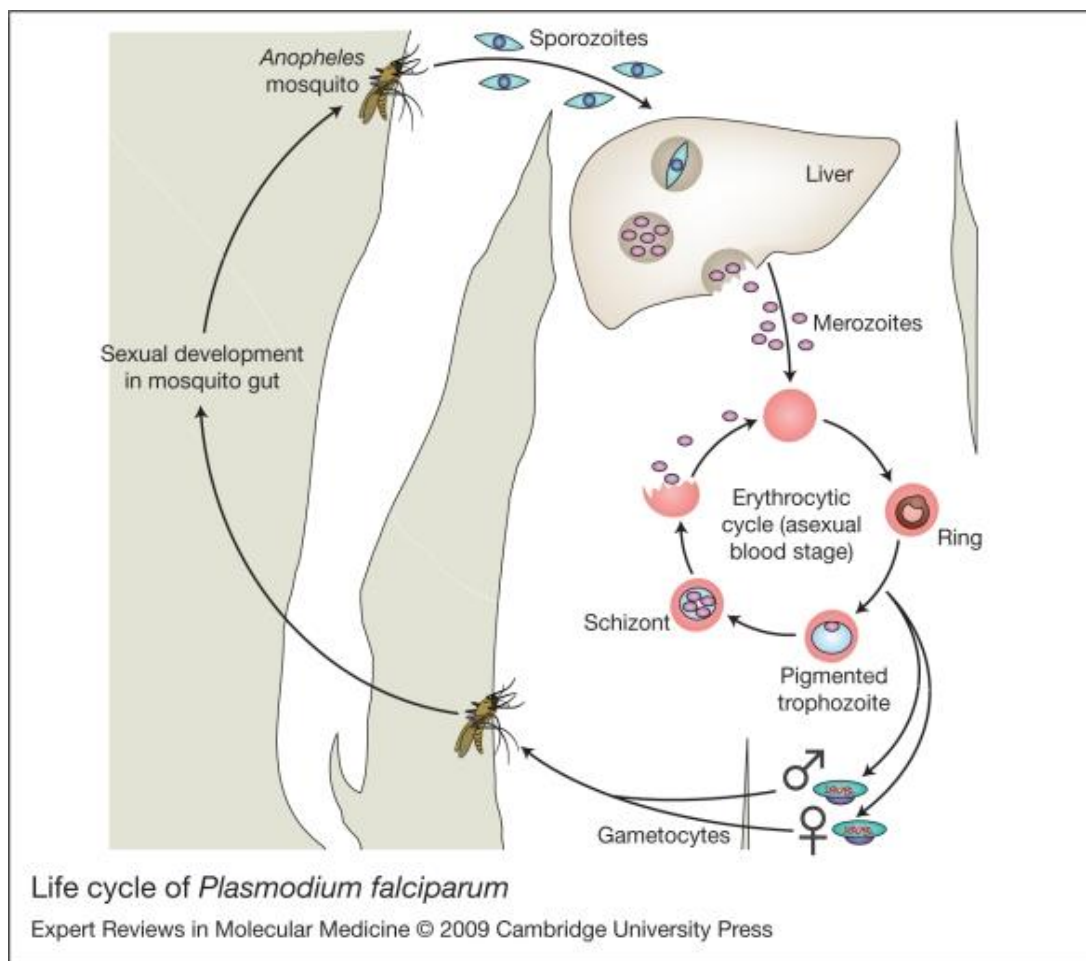


Figure 1: Life cycle of *P. falciparum*.

The work described in this thesis focuses largely on the asexual blood stage, with some discussion of gametocytes as well. This figure was originally published by Rowe and colleagues here¹⁵. No changes were made. The Creative Commons Attribution-NonCommercial-ShareAlike copyright license information can be found from the PMC full text link which is on the cited PubMed page.

P. falciparum and the rest of the *Plasmodium* genus are members of the Apicomplexa phylum, a group of parasites also home to the organisms causing Toxoplasmosis and Babesiosis, among others. Apicomplexa parasites are eukaryotic and are defined by the presence of an apical complex which allows for cellular attachment and invasion during their life cycle. Many Apicomplexa also possess an organelle

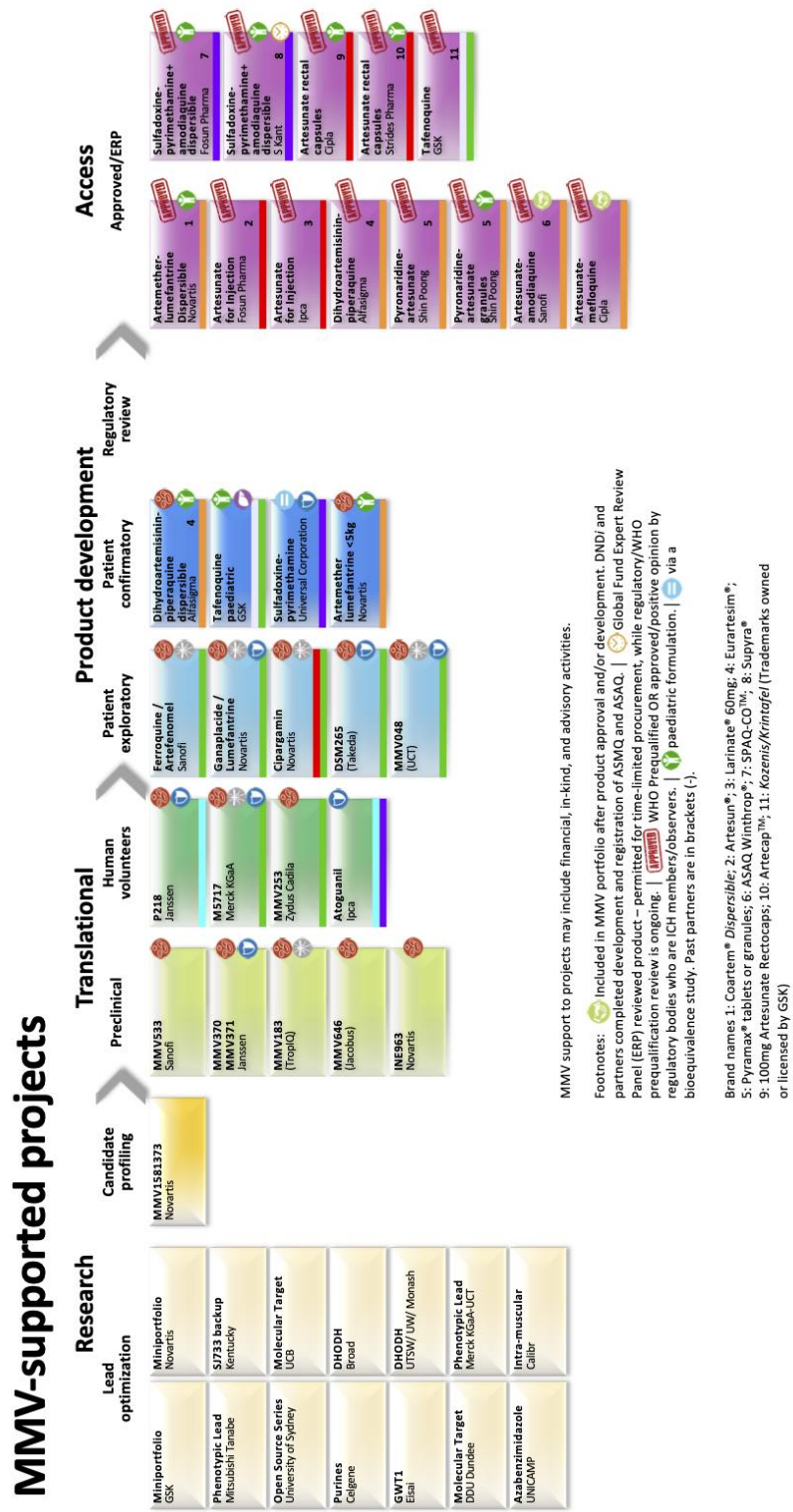
called the apicoplast, which is essential to *P. falciparum*. A full review of the apicoplast can be found here¹⁶, it has characteristics of prokaryotic organisms and is similar to plant and algal plastids. Due to these similarities to prokaryotes, it is mentioned that some common antibiotics are effective against the apicoplast¹⁶. Of particular importance is noting that since hosts (humans) are obviously not prokaryotic, aspects of the apicoplast can be exploited to develop drugs that are extremely selective for just the parasite.

Chapter 2

Investigating Interactions Between SJ733 and P218

Background

Combinations of drugs have been explored to treat illness since the middle of the 20th century, with notable examples including treatment of tuberculosis with streptomycin and para-aminosalicylic acid in 1950¹⁷, and an experiment into a combination therapy for childhood leukemia in 1965¹⁸. Arguments for the use of combination therapies in the treatment of malaria have been made for over twenty years¹⁹. As early as 2004, when resistance to all classes of antimalarials except the artemisinin's had been seen, combination therapies were suggested as a means of delaying the then-unseen rise of resistance against artemisinin's⁹. Now that resistance to artemisinin has been identified in the field and has been studied to a fair degree (see review here¹⁰), we find ourselves with no remaining 100% resistance-free options for the treatment of patients. Thus, the design of future therapies demands great care to ensure these treatments are effective and avoid resistance development. While current therapeutics are in danger, this is not to say that we are completely at a loss in terms of drug development. The Medicines for Malaria Venture (MMV), a nonprofit founded in 1999, has spearheaded public-private partnerships for decades to help identify new promising new antimalarials. In 2016 a massive study was published compiling the results of 55 laboratories who studied 400 representative compounds from the "Malaria Box," a free resource from MMV intended to drive open source antimalarial drug discovery²⁰. The results not only helped characterize potential antimalarials, but also helped identify compounds which could kill other pathogens as well. As of April 23, 2020, MMV continues to support 33 projects in the drug development pipeline (undergoing research, translational or product development work), while 13 have been "WHO prequalified or approved/positive opinion by regulatory bodies who are ICH members/observers²¹."



December 2019



Figure 2: MMV Supported Projects

Projects supported by MMV as of December 2019 are shown. This figure was obtained from the MMV website²¹. It is worth noting that many of the therapies further along in development are combination therapies, with artemisinin or one of its derivatives often used as a component drug.

Combination therapies comprised of drugs targeting different parts of an organism's metabolism represent a valuable means of slowing the development of resistance for an intuitive reason. It is less probable for two independent, unrelated mutations to arise simultaneously and provide resistance to a combination of drugs with different targets than it would be for an organism to spontaneously generate one mutation for a monotherapy (or a combination that could be overcome with a single mutation). The basis for this idea was discussed in the context of malaria by Nicholas White in 1998²². Moreover, a seemingly unrelated but desirable property of combination therapies is that the drugs comprising the therapy be synergistic (that is, they augment each other's activity to more efficiently eliminate the parasite). A noted advantage of such combinations is that they can allow for effective parasite clearance while keeping dosage low, reducing the potential for side effects²³. On the opposite end of the spectrum, partner drugs which antagonize each other (reduce each other's efficacy) are largely not attractive as they may suffer the opposite effect, raising the required dosage and increasing side effects. The most notable example of a synergistic pairing of antimalarials is that of atovaquone and proguanil, the component drugs of Malarone. While proguanil is not particularly effective on its own, it is thought to enhance atovaquone efficacy by aiding atovaquone-driven collapse of the parasite's mitochondrial membrane potential²⁴. Atovaquone achieves this collapse via inhibition of the transfer of electrons from ubiquinone to cytochrome *bc₁*, disrupting the parasite's mitochondrial electron transport chain (see here for a more complete discussion²⁵). It also inhibits enzymes involved in pyrimidine biosynthesis as a downstream effect, and as a result its use results in a buildup of *N*-carbamoyl-L-aspartate and dihydroorotate, both pyrimidine precursors, in the parasite²⁶.

Taken together, the ideal antimalarial combination therapy is one in which the component drugs target independent aspects of the parasite's metabolism while also synergizing with each other. As such combinations are rather unintuitive, it is difficult to envision how one might predict what partner drugs may comprise such an idealistic pair. In the absence of specific pairings to try, a high-throughput screen strategy has been carried out to find interactions between antimalarials²⁷.

Defining whether or not two drugs interact, and identifying what type of interaction exists, is typically done via an isobologram which is described by succinctly by Angus Bell here²³. In short, drugs are tested in varying combinations and the half-maximal inhibitory concentration (IC_{50}) of each drug in a given combination is graphed on a simple x-y coordinate system. That is, each single combination of drugs yields an IC_{50} for both drugs individually, and those values are plotted as (IC_{50} Drug A, IC_{50} Drug B). In this example, the X-axis would indicate concentrations of Drug A, and the Y-axis would indicate concentrations of Drug B. The X- and Y-intercepts would be the IC_{50} value of the respective drugs when used alone. These values can also be plotted as fractional IC_{50} s (FIC₅₀s), which according to Bell are defined as “the concentration of inhibitor present in the combination divided by the concentration of inhibitor alone that gives the same effect.”²³ If an additive interaction (i.e. neither synergistic nor antagonistic) was seen between Drugs A and B, the expected isobole would be a straight line connecting the intercepts. If the experimentally-determined isobole curves in towards the origin, this is indicative of synergy. This is because points below the additive isobole indicate that less of each drug was required to achieve the same level of effect than the amount of each drug which would have been expected to achieve that effect with an additive interaction. Conversely, bowing out away from the origin indicates antagonism for a similar reason.

Objectively determining antagonism and synergism from isobolograms is not simple. As Bell discusses, common thresholds based on the sum of the FIC₅₀s at the middle of the isobologram are that less than 0.5 indicates synergism, and greater than 2 or 4 indicates antagonism²³. However, as Bell points out, these are arbitrary. Software does exist to perform more sophisticated data analysis, such as

CalcuSyn, which ultimately defines synergism and antagonism based on the combination index which is defined similarly to the summed FIC50s. Such software has been used to study antimalarials²⁸.

Here, I contribute my own analysis of two antimalarials which at the time of experimental planning were in the drug development pipeline and supported by the Medicines for Malaria Venture. I chose to focus on two compounds which were already in the pipeline due to their demonstrated potential as treatments and the existing investment in each, though to the best of my knowledge the two had not been tried as a pair.

The first of the two compounds, (+)-SJ733 (hereafter referred to as SJ733), has been characterized as an inhibitor of the *P. falciparum* sodium cation transporter PfATP4²⁹. *In vivo* experiments with *P. falciparum* indicate that SJ733 acts at dosages on par with or better than some existing antimalarials and is capable of preventing transmission of *P. berghei* to mosquitoes²⁹. Promisingly, although resistant strains could readily be selected for *in vitro*, *P. falciparum* mutants resistant to the same class of compounds suffered fitness costs compared to parental strains and development of *P. berghei* resistance to a close analog of SJ733 *in vivo* was slow and weak²⁹. Prior *in vitro* metabolomics experiments conducted on parasite extracts from SJ733-treated parasites has shown that parasites treated with SJ733 have decreased levels of pyrimidine precursors, peptides, and nucleotides with some increase of deoxynucleotides (see Figure 3 below)²⁶. Very recently, the findings of a phase 1a/b first-in-human and induced blood-stage malaria trial conducted for SJ733 was published³⁰, as was a short review of the compound and the outcomes of this new trial in the context of other ATP4 inhibitors³¹. In summary, parasite clearance was slower than another in-development ATP4 inhibitor but on par with an artemisinin derivative. The drug was found to be safe to patients, with few adverse events thought to have occurred due to SJ733 rather than malaria. The authors of the trial were ultimately optimistic about SJ733's continued development as part of a future combination therapy.

The second compound, P218, is a pyrimidine molecule with a flexible side chain which was developed through a target enzyme structure-based design process seeking to improve upon compounds

targeting *P. falciparum* dihydrofolate reductase (PfDHFR) to which resistance has arisen (particularly, pyrimethamine³²). P218 is also a PfDHFR inhibitor but is of interest for its efficacy in inhibiting both wildtype *P. falciparum* and a PYR-resistant quadruple mutant *P. falciparum* strain *in vitro*, with more proven efficacy *in vivo*³². Prior *in vitro* metabolomics experiments conducted on parasite extracts from P218-treated parasites has shown that parasites treated with P218 have sharply increased metabolites involved in folate biosynthesis, with a decrease in those involved in central carbon metabolism/cofactors (see Figure 3 below)²⁶. Additionally, resistance against P218 is expected to be slowed as mutations that would block P218 binding are expected to also interfere with substrate binding by PfDHFR, since P218 binds similarly to the normal enzyme substrate³².

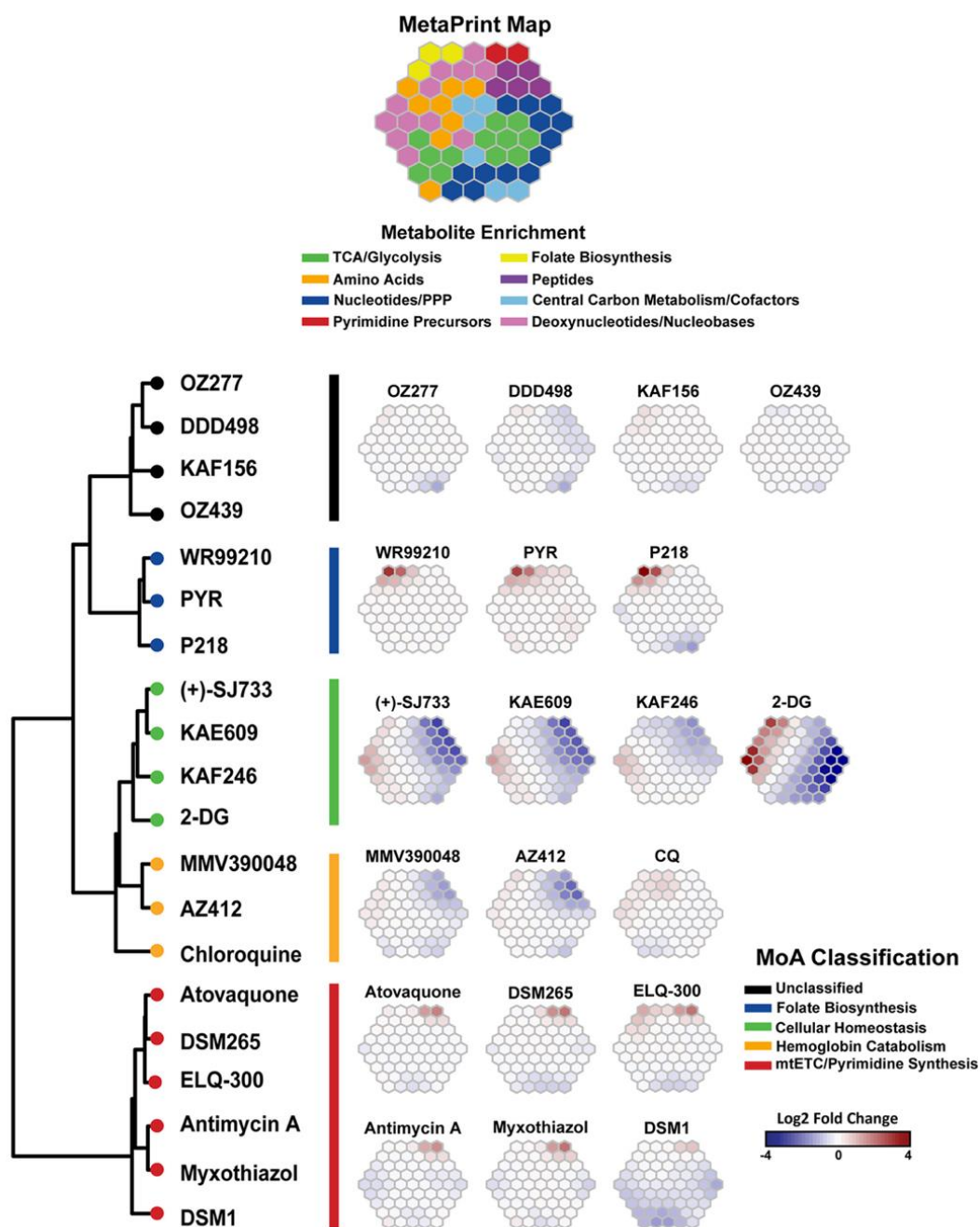


Figure 3: Prior Metabolomic Fingerprint Analysis of SJ733 and P218 by the Llinás Lab

This figure was adapted from Allman et al 2016²⁶, which was prior work performed in our lab.

The clustered compounds shown were classified by their mode of action based on changes in metabolites compared to a no-drug control. This analysis leveraged self-organizing maps displayed on the hexagonal plots shown at the top of the figure, known as metaprints. Metabolites in each smaller hexagon were

categorized by their known metabolic pathways according to the KEGG database, allowing for visualization of how the parasite's metabolism changed due to each drug. P218 and SJ733 have very different metaprints, supporting the knowledge that they likely act on very different parts of the parasite's metabolism.

Based on experimental efficacy and likelihood for resistance, SJ733 and P218 have appealing characteristics as prospective antimalarials. Since the two compounds are promising and have different targets in the parasite's metabolism, they could make good partner drugs in a therapy pending drug-drug interactions. Consequently, their combination was investigated to look for potential drug-drug interactions. Half-maximal inhibitory concentration (IC_{50}) values were first determined for each drug independently via a SYBR Green assay to help guide planning of the combination experiment, and a fixed-ratio SYBR Green assay (derived from the publication here³³) in conjunction with isobologram analysis was employed to evaluate potential drug-drug interactions.

Materials and Methods

For each experiment, 96-well plates were prepared as depicted in the plate layouts below. All drug-containing or no-drug wells contained 100 μL of drug media (or RPMI for the no-drug wells) and 100 μL of approximately 0.1% parasitemia (mostly ring-stage), 1% final hematocrit culture (except plate sets 2 and 3 of the combination experiments, which had 0.5% final hematocrit).

For the individual P218 experiment, drug dilutions were prepared outside the plate and 100 μL of the various drug media was aliquoted into their respective wells. For the individual SJ733 experiment, atovaquone drug dilutions were prepared outside the plate and 100 μL were aliquoted into their respective wells, but SJ733 was serially diluted directly in the wells. This was done by aliquoting 200 μL of two times the highest desired final concentration of drug into the first well and aliquoting 100 μL of RPMI into the rest of the wells in that row. 100 μL of drug media was transferred to the next adjacent well, mixed, and transferred to the next well, with a change of pipet tips in-between. This continued until the last well, where following mixing, 100 μL of media was discarded. This resulted in two-fold serially diluted SJ733, which would reach their desired concentrations after the addition of 100 μL of culture.

For the combination experiments, conical tubes containing four times the desired maximum concentration of drug in each solution (i.e. one SJ733-containing RPMI and one P218-containing RPMI tube per solution, for solutions 1-6) were first generated. The appropriate partner tubes for each solution (1-6) were then combined, resulting in solutions 1-6 with two times the desired maximum concentration. For solutions 1 and 6, RPMI was used in place of drug media for the P218 and SJ733 tubes, respectively, since solution 1 contained no P218 and solution 6 contained no SJ733. The solutions were then serially diluted in the 96 well plate as described before for SJ733, resulting in two-fold serially diluted drug media that was still two times the desired final concentration. The final addition of culture to these wells brought the solutions to their desired final concentration. No-drug controls used 100 μL of RPMI in place of drug media. RPMI controls contained 200 μL of RPMI, with no culture in the wells. The maximum amount of DMSO in any drug-containing well was 0.06%.

Following plate preparation, plates were incubated under regular gas and temperature conditions for 72 hours. The individual P218 experiment also had 100 μ L of sample withdrawn from each well after 48 hours. After incubation, plates were frozen at -80°C . For analysis, SYBR Green was diluted in lysis buffer at 0.4 μ L of SYBR Green per 1 mL of total buffer volume needed. Sample plates were thawed, and wells were mixed before pipetting 100 μ L of each well into the same position in a clean ceramic 96 well plate. 100 μ L of buffered SYBR Green was also added to each well in the ceramic plate and mixed. Plates were then wrapped in foil and incubated at normal gas/temperature conditions for 2 hours. Fluorescence within each well was then read on a microplate reader (Biotek, Winooski, VT) and the resulting data was exported to Excel and GraphPad Prism³⁴ for Mac (GraphPad Software, San Diego, California USA, Versions 7 and 8.4.2 were used) for further analysis. Methodology for the generation of each figure can be found in the corresponding figure legend.

Parasites used in these experiments were presumed mycoplasma free. The parasites used came from a lab stock of MR4, mycoplasma-free, 3D7 parasites that was thawed on October 25, 2018. The same line was passaged and used for the individual P218 experiment on October 27, 2018. The remaining culture was split and passaged further and was split into three cultures on November 5, 2018, which were all continued. One of these three cultures was used for the individual SJ733 experiment and the first SJ733/P218 combination experiment on November 9, 2018. It and the other three cultures were continued and frozen at the same time in the following several days. One of these cultures, not the same one used in the November 9 experiment, was thawed and continued on November 26, 2018 until it was frozen on December 18, 2018. A stock of that same December 18 culture was then thawed on January 8, 2019 and was ultimately used for the SJ733/P218 replicate experiments on February 6, 2019. The leftover culture was split and continued and tested mycoplasma free on February 27, 2019. Thus, we can safely presume the parasites used for the October 27, 2018 and February 6, 2019 experiments were mycoplasma free, as that line tested mycoplasma free. The parasites used on November 9, 2018 were split from a parent culture that can be presumed mycoplasma free on November 5, 2018, and were used just four days later.

This short time after splitting combined with the similarity of the results from those experiments with the others in this study make it unlikely that mycoplasma contamination was picked up by November 9, 2018. Other culture splits which were not explicitly stated took place during this time, but this documentation focuses on lines used in experiments.

SJ733 and P218 stocks were provided courtesy of Erik Allman and Jeremy Burrows. Atovaquone was purchased from Sigma (#A7986-50mg).

Eight total 96 well plates were prepared to measure IC50 values: one each for the individual drugs, and three sets of two plates for combination experiments. The combination experiments had the same design, so the plate setup is only shown once. Replicates 2 and 3 of the combination experiments were performed at the same time with the same starting culture and as such represent only one additional biological replicate, but with six technical replicates for each solution between the two sets of plates.

	A	B	C	D	E	F	G	H	
1	0.0008 nM	0.004 nM	0.02 nM	0.1 nM	0.5 nM	2.5 nM	12.5 nM	62.5 nM	ATV1
2	0.0008 nM	0.004 nM	0.02 nM	0.1 nM	0.5 nM	2.5 nM	12.5 nM	62.5 nM	ATV2
3	0.0008 nM	0.004 nM	0.02 nM	0.1 nM	0.5 nM	2.5 nM	12.5 nM	62.5 nM	ATV3
4	0.0081 nM	0.0243 nM	0.073 nM	0.22 nM	0.66 nM	2 nM	6 nM	18 nM	P1
5	0.0081 nM	0.0243 nM	0.073 nM	0.22 nM	0.66 nM	2 nM	6 nM	18 nM	P2
6	0.0081 nM	0.0243 nM	0.073 nM	0.22 nM	0.66 nM	2 nM	6 nM	18 nM	P3
7	--	--	--	--	--	--	--	--	ND1
8	--	--	--	--	--	--	--	--	ND2
9	--	--	--	--	--	--	--	--	ND3
10	--	--	--	--	--	--	--	--	RPMI1
11	--	--	--	--	--	--	--	--	RPMI2
12	--	--	--	--	--	--	--	--	RPMI3

Figure 4: 96 Well Plate Layout for the Determination of the IC₅₀ of P218

Concentration values within cells refer to the final concentration of drug within that well. Tan wells refer to no-drug controls which contained 100 μ L of 0.25% Albumax RPMI in place of any drug media. Light red wells refer to RPMI control wells which contained 200 μ L of 0.25% Albumax RPMI with no culture or drug added. Abbreviations: ATV, Atovaquone; P, P218; ND, no drug.

	A	B	C	D	E	F	G	H	
1	0.0008 nM	0.004 nM	0.02 nM	0.1 nM	0.5 nM	2.5 nM	12.5 nM	62.5 nM	ATV1
2	0.0008 nM	0.004 nM	0.02 nM	0.1 nM	0.5 nM	2.5 nM	12.5 nM	62.5 nM	ATV2
3	0.0008 nM	0.004 nM	0.02 nM	0.1 nM	0.5 nM	2.5 nM	12.5 nM	62.5 nM	ATV3
4	1.875 nM	3.75 nM	7.5 nM	15 nM	30 nM	60 nM	120 nM	240 nM	SJ1
5	1.875 nM	3.75 nM	7.5 nM	15 nM	30 nM	60 nM	120 nM	240 nM	SJ2
6	1.875 nM	3.75 nM	7.5 nM	15 nM	30 nM	60 nM	120 nM	240 nM	SJ3
7	--	--	--	--	--	--	--	--	ND1
8	--	--	--	--	--	--	--	--	ND2
9	--	--	--	--	--	--	--	--	ND3
10	--	--	--	--	--	--	--	--	RPMI1
11	--	--	--	--	--	--	--	--	RPMI2
12	--	--	--	--	--	--	--	--	RPMI3

Figure 5: 96 Well Plate Layout for the Determination of the IC₅₀ of SJ733

Concentration values within cells refer to the final concentration of drug within that well. Tan wells refer to no-drug controls which contained 100 μ L of 0.25% Albumax RPMI in place of any drug media. Light red wells refer to RPMI control wells which contained 200 μ L of 0.25% Albumax RPMI with no culture or drug added. Abbreviations: ATV, Atovaquone; SJ, SJ733; ND, no drug.

	A	B	C	D	E	F	G	H	
1									RPMI
2									ND
3		SOLN 1: 0.015625	SOLN 1: 0.03125	SOLN 1: 0.0625	SOLN 1: 0.125	SOLN 1: 0.25	SOLN 1: 0.5	SOLN 1: FULL	
4		SOLN 1: 0.015625	SOLN 1: 0.03125	SOLN 1: 0.0625	SOLN 1: 0.125	SOLN 1: 0.25	SOLN 1: 0.5	SOLN 1: FULL	
5		SOLN 1: 0.015625	SOLN 1: 0.03125	SOLN 1: 0.0625	SOLN 1: 0.125	SOLN 1: 0.25	SOLN 1: 0.5	SOLN 1: FULL	
6		SOLN 2: 0.015625	SOLN 2: 0.03125	SOLN 2: 0.0625	SOLN 2: 0.125	SOLN 2: 0.25	SOLN 2: 0.5	SOLN 2: FULL	
7		SOLN 2: 0.015625	SOLN 2: 0.03125	SOLN 2: 0.0625	SOLN 2: 0.125	SOLN 2: 0.25	SOLN 2: 0.5	SOLN 2: FULL	
8		SOLN 2: 0.015625	SOLN 2: 0.03125	SOLN 2: 0.0625	SOLN 2: 0.125	SOLN 2: 0.25	SOLN 2: 0.5	SOLN 2: FULL	
9		SOLN 3: 0.015625	SOLN 3: 0.03125	SOLN 3: 0.0625	SOLN 3: 0.125	SOLN 3: 0.25	SOLN 3: 0.5	SOLN 3: FULL	
10		SOLN 3: 0.015625	SOLN 3: 0.03125	SOLN 3: 0.0625	SOLN 3: 0.125	SOLN 3: 0.25	SOLN 3: 0.5	SOLN 3: FULL	
11		SOLN 3: 0.015625	SOLN 3: 0.03125	SOLN 3: 0.0625	SOLN 3: 0.125	SOLN 3: 0.25	SOLN 3: 0.5	SOLN 3: FULL	
12									ND

	A	B	C	D	E	F	G	H	
1									RPMI
2									ND
3		SOLN 4: 0.015625	SOLN 4: 0.03125	SOLN 4: 0.0625	SOLN 4: 0.125	SOLN 4: 0.25	SOLN 4: 0.5	SOLN 4: FULL	
4		SOLN 4: 0.015625	SOLN 4: 0.03125	SOLN 4: 0.0625	SOLN 4: 0.125	SOLN 4: 0.25	SOLN 4: 0.5	SOLN 4: FULL	
5		SOLN 4: 0.015625	SOLN 4: 0.03125	SOLN 4: 0.0625	SOLN 4: 0.125	SOLN 4: 0.25	SOLN 4: 0.5	SOLN 4: FULL	
6		SOLN 5: 0.015625	SOLN 5: 0.03125	SOLN 5: 0.0625	SOLN 5: 0.125	SOLN 5: 0.25	SOLN 5: 0.5	SOLN 5: FULL	
7		SOLN 5: 0.015625	SOLN 5: 0.03125	SOLN 5: 0.0625	SOLN 5: 0.125	SOLN 5: 0.25	SOLN 5: 0.5	SOLN 5: FULL	
8		SOLN 5: 0.015625	SOLN 5: 0.03125	SOLN 5: 0.0625	SOLN 5: 0.125	SOLN 5: 0.25	SOLN 5: 0.5	SOLN 5: FULL	
9		SOLN 6: 0.015625	SOLN 6: 0.03125	SOLN 6: 0.0625	SOLN 6: 0.125	SOLN 6: 0.25	SOLN 6: 0.5	SOLN 6: FULL	
10		SOLN 6: 0.015625	SOLN 6: 0.03125	SOLN 6: 0.0625	SOLN 6: 0.125	SOLN 6: 0.25	SOLN 6: 0.5	SOLN 6: FULL	
11		SOLN 6: 0.015625	SOLN 6: 0.03125	SOLN 6: 0.0625	SOLN 6: 0.125	SOLN 6: 0.25	SOLN 6: 0.5	SOLN 6: FULL	
12									ND

Figure 6: 96 Well Plate Layouts for the Investigation of Interactions Between P218 and SJ733

Numerical values within wells refer to the proportional concentration of that well's drugs to the full solution in column H. For example, well G3 in the top plate contains 0.5 times the concentration of drug in well H3 due to a single twofold dilution. Tan wells refer to no-drug controls which contained 100 μ L of 0.25% Albumax RPMI in place of any drug media. Light red wells refer to RPMI control wells which contained 200 μ L of 0.25% Albumax RPMI with no culture or drug added. Abbreviations: SOLN, solution. See Table 1 for contents of each solution.

Table 1: Concentrations of SJ733 and P218 in Solutions 1 Through 6

Solution Number	Concentration of SJ733 [nM]	Concentration of P218 [nM]
1	280	0
2	224	0.64
3	168	1.28
4	112	1.92
5	56	2.56
6	0	3.2

SJ733 and P218 were varied at fixed ratios across six solutions. Listed concentrations refer to the final concentration of SJ733 and P218 after 100 μ L of each solution was combined with 100 μ L of parasite culture in the 96 well plate. In other words, the prepared solutions were two-fold more concentrated before mixing with culture in the plates took place.

Results

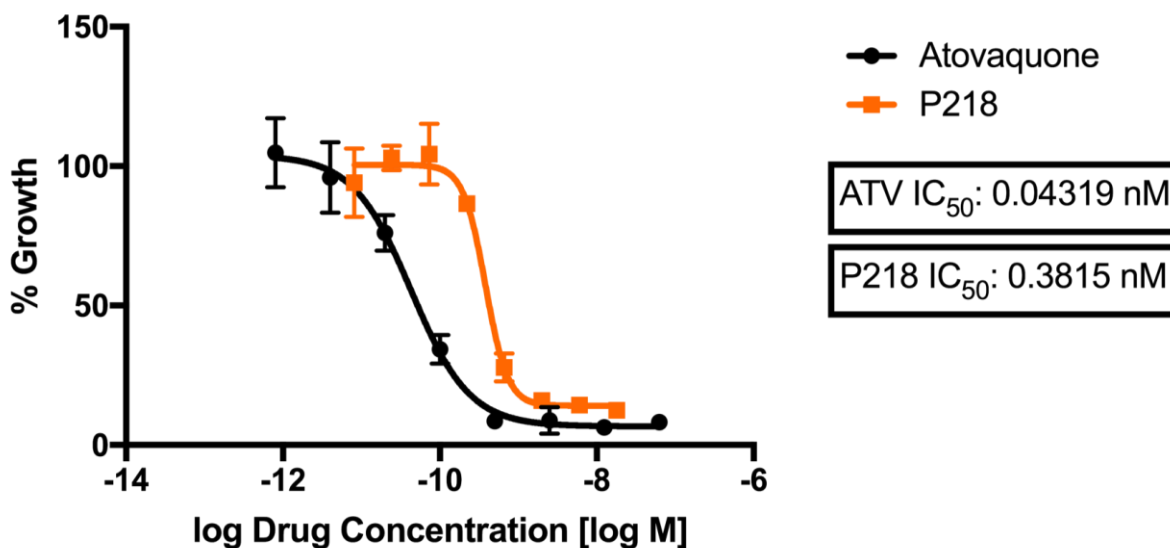


Figure 7: IC₅₀ Determination of P218

Fluorescence intensity readout was normalized by subtracting the average of the RPMI control readout from each sample readout and setting 0% growth equal to 0 intensity. 100% growth was set to the average of the blank-subtracted no-drug control readout. Each of the three technical replicates in the plate was normalized separately. The normalized intensity was plotted against corresponding log-transformed drug concentrations and a curve was fitted via a log(inhibitor) vs. response – Variable slope (four parameters) model in GraphPad Prism, from which the IC₅₀ values were derived. Error bars represent the standard deviation of three technical replicate wells at each drug concentration.

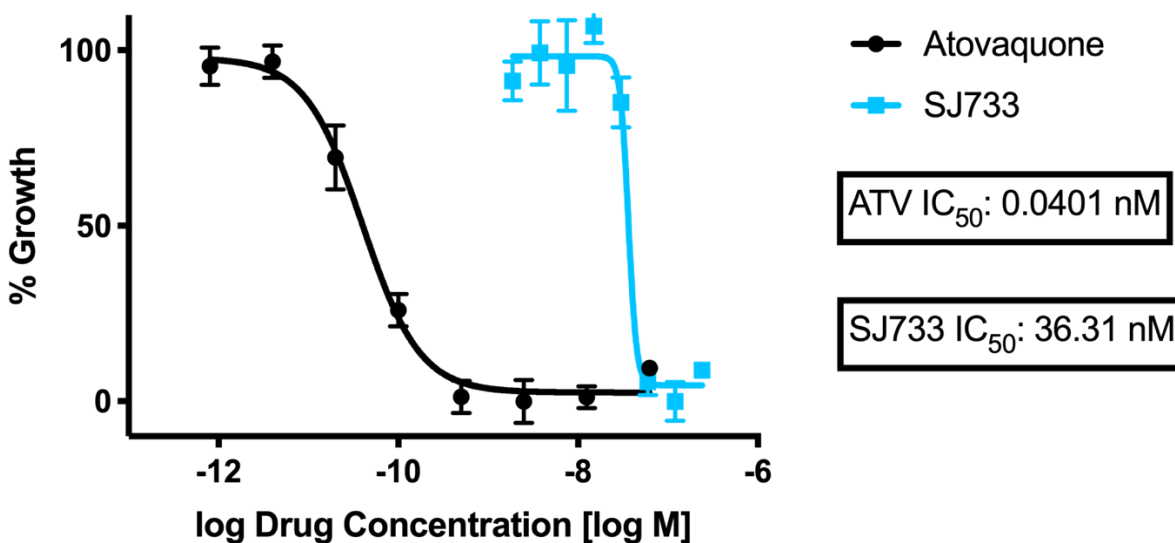


Figure 8: IC₅₀ Determination of SJ733

Due to an abnormally high RPMI control reading, fluorescence intensity readout was normalized by defining 0% growth as the smallest mean (of three technical replicates) for each drug. This makes growth relative to the lowest amount of signal as opposite to an absolute measurement. 100% growth was defined as the average of the no-drug control readout. The three technical replicates for each drug were first averaged, and the means were normalized. The normalized intensity was plotted against corresponding log-transformed drug concentrations and a curve was fitted via a log(inhibitor) vs. response – Variable slope (four parameters) model in GraphPad Prism, from which the IC₅₀ values were derived. Error bars represent the standard deviation of three technical replicate wells at each drug concentration.

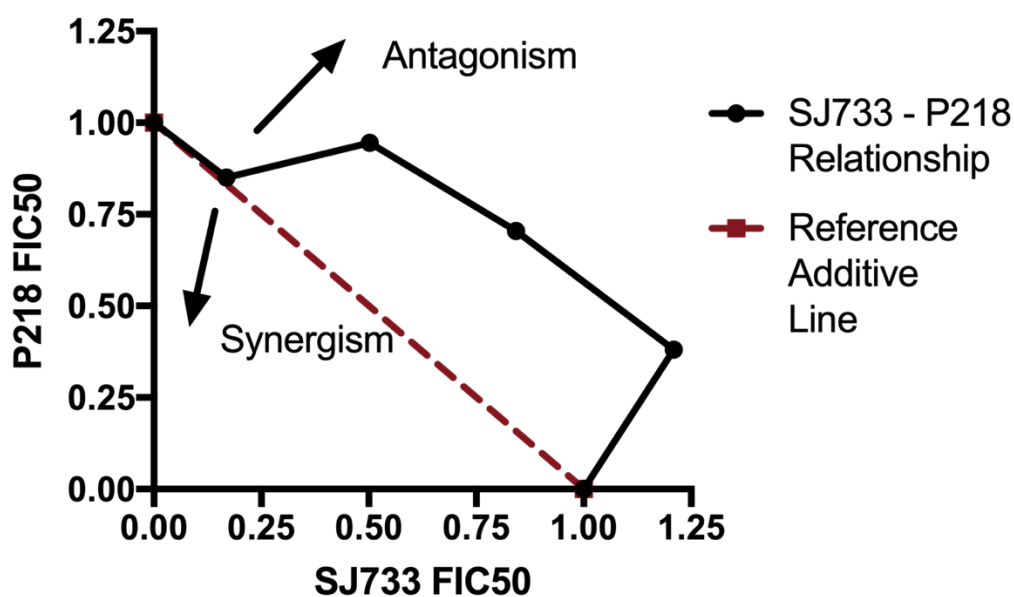


Figure 9: Isobologram Analysis of First Set of SJ733 – P218 Combination Plates

Isobologram construction was performed by normalizing each technical replicate for each solution separately, with 0% defined as the smallest value in each subcolumn and 100% defined as the largest value in each subcolumn. No blank subtraction or no drug thresholding was performed. Normalized values were then fit to log-transformed drug concentrations for both SJ733 and P218 using a $\log(\text{inhibitor})$ vs. response – Variable slope (four parameters) fit, resulting in 5 fitted curves for each drug. IC_{50} values were calculated from these curves by GraphPad Prism, and were used to determine FIC₅₀ values for each drug for each solution. Plotted points represent best-fit values for each drug's FIC₅₀ for all six solutions (e.g. the point at (0, 1) represents solution 6, the point at approximately (0.2, 0.85) represents solution 5, and so on). The connecting line does not represent a model, it is simply a connecting line. The dashed line represents the expected interaction for two drugs which do not interact (i.e. are additive), with deviations above the line suggesting antagonism and deviations below the line suggesting synergism.

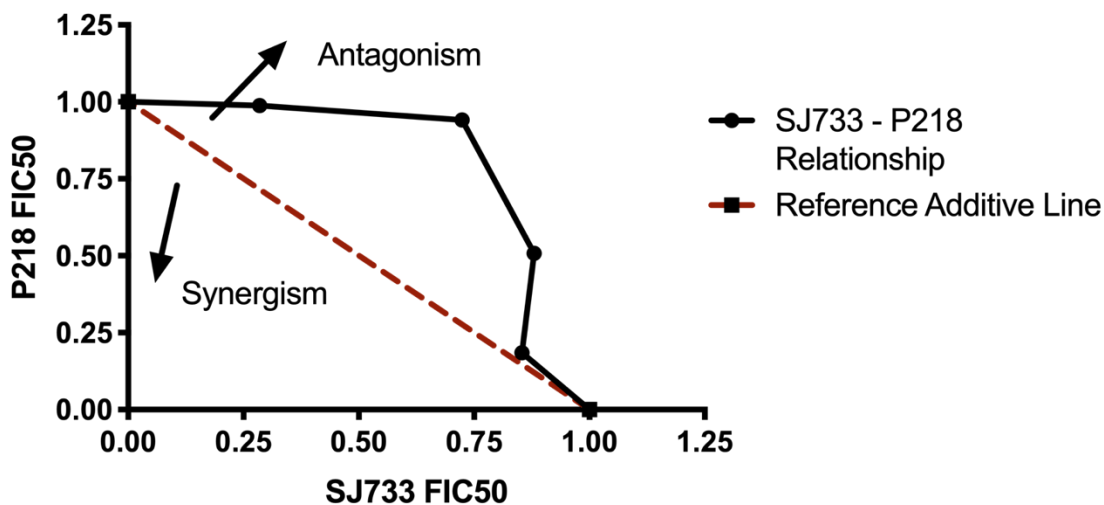


Figure 10: Isobologram Analysis of Second Set of SJ733 – P218 Combination Plates

This figure was constructed in the same way as previously described, but using data from the first replicate set of plates for the SJ733 and P218 combination. It should be noted that this set of plates was generated at the same time and with the same input culture as the third set of plates, meaning they are not truly distinct biological replicates.

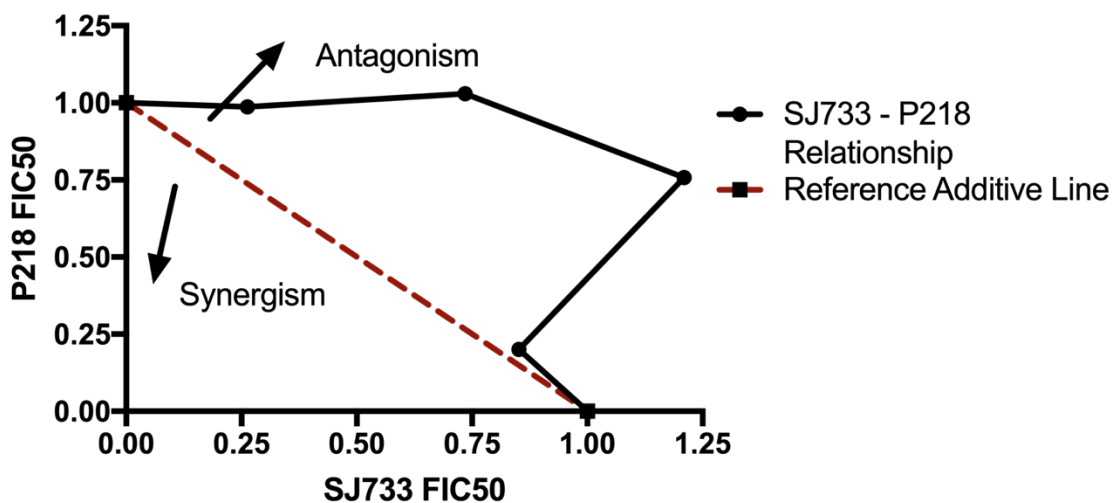


Figure 11: Isobologram Analysis of Third Set of SJ733 – P218 Combination Plates

This figure was constructed in the same way as previously described, but using data from the second replicate set of plates for the SJ733 and P218 combination. It should be noted that this set of plates was generated at the same time and with the same input culture as the second set of plates, meaning they are not truly distinct biological replicates.

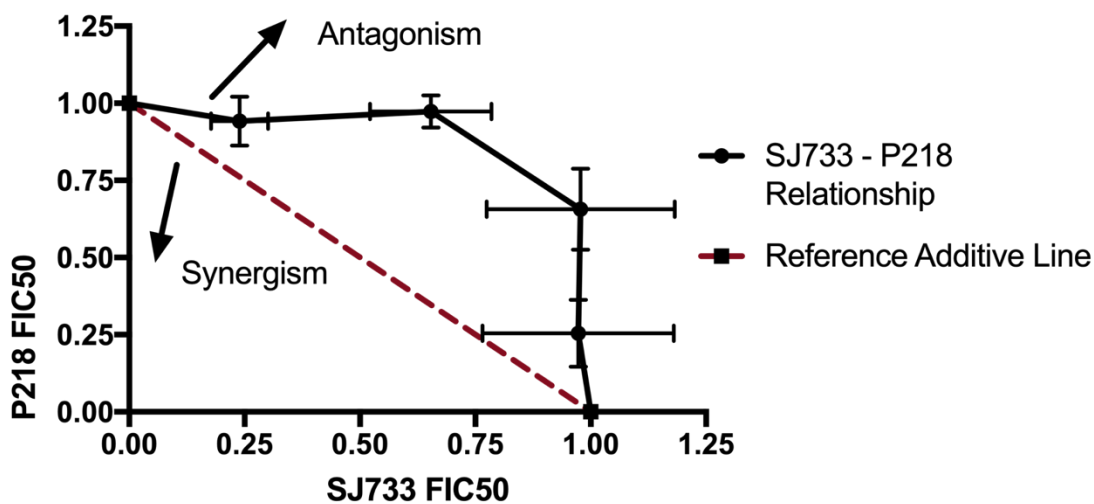


Figure 12: Combined Isobologram Analyses of SJ733 – P218 Combination Plates

Data from the three sets of plates were combined into a single isobologram, with data points representing the average of the three FIC₅₀ values for each drug (calculated using the best-fit IC₅₀ values within each plate), from each of the solutions in the previous plate sets, with error bars representing the standard deviation derived from this average plotted for both drugs at each solution. It should be noted that since the second and third set of plates were generated at the same time with the same input culture, although three sets of plates worth of data are represented, these data only comprise two biological replicates.

Table 2: IC₅₀ Values For Individual Drugs and Combination Replicates

Drug & Solution	IC ₅₀ Plate Set 1 (M)	IC ₅₀ Plate Set 2 (M)	IC ₅₀ Plate Set 3 (M)
SJ733 Alone	3.6e-008*	N/A, single plate	N/A, single plate
P218 Alone	3.8e-010	N/A, single plate	N/A, single plate
SJ733 Solution 1	4.3e-008*	3.5e-008 ⁺	3.4e-008 ⁺
SJ733 Solution 2	5.2e-008 ⁺	3.0e-008 ⁺	2.9e-008 ⁺
SJ733 Solution 3	3.6e-008	3.1e-008 [%]	4.1e-008 ⁺
SJ733 Solution 4	2.2e-008 [%]	2.6e-008	2.5e-008*
SJ733 Solution 5	7.3e-009	1.0e-008*	8.8e-009*
SJ733 Solution 6	N/A (no SJ in solution)	N/A (no SJ in solution)	N/A (no SJ in solution)
P218 Solution 1	N/A (no P218 in solution)	N/A (no P218 in solution)	N/A (no P218 in solution)
P218 Solution 2	1.5e-010 ⁺	8.6e-011 ⁺	8.2e-011 ⁺
P218 Solution 3	2.8e-010	2.4e-010 [%]	3.1e-010 ⁺
P218 Solution 4	3.7e-010 [%]	4.4e-010	4.2e-010*
P218 Solution 5	3.3e-010	4.6e-010*	4.0e-010*
P218 Solution 6	3.9e-010 ⁺	4.6e-010*	4.1e-010

Best-fit IC₅₀ values derived from GraphPad Prism for individual drugs and all solutions across the three sets of plates tested. Plate sets 2 and 3 were derived from the same starter culture and as such cannot be considered biological replicates. Notes for statistical errors: * = lacking one side of a 95% confidence interval. % = lacking both sides of a 95% confidence interval. ⁺ = nonlinear fit flagged “ambiguous” by GraphPad Prism, so confidence intervals are not given.

Table 3: Derived FIC50 Values

Drug & Solution	FIC50 (Plate Set 1)	FIC50 (Plate Set 2)	FIC50 (Plate Set 3)
SJ733 Solution 1	1.0	1.0	1.0
SJ733 Solution 2	1.2	0.85	0.85
SJ733 Solution 3	0.84	0.88	1.2
SJ733 Solution 4	0.50	0.72	0.73
SJ733 Solution 5	0.17	0.29	0.26
SJ733 Solution 6	0 (no SJ733 in solution)	0 (no SJ733 in solution)	0 (no SJ733 in solution)
P218 Solution 1	0 (no P218 in solution)	0 (no P218 in solution)	0 (no P218 in solution)
P218 Solution 2	0.38	0.18	0.20
P218 Solution 3	0.71	0.51	0.76
P218 Solution 4	0.95	0.94	1.0
P218 Solution 5	0.85	0.99	0.99
P218 Solution 6	1.0	1.0	1.0

FIC50 values were derived for each drug combination point by dividing the drug's IC_{50} value in that combination by the calculated IC_{50} of the drug alone within the same plate. For example, the FIC50 of SJ733 in Plate Set 1, Solution 2, is equal to $5.2e-008$ (the IC_{50} of SJ733 in solution 2 for plate set 1) divided by $4.3e-008$ (the IC_{50} of SJ733 in solution 1, which only contained SJ733). For P218, solution 6 served as the reference IC_{50} in each plate since solution 6 contained only P218. By definition, the FIC50 values for drugs when alone are 1, or 0 if they are not present in the solution. Calculations were performed with the full IC_{50} values from GraphPad prism.

Table 4: Mean FIC50 Values

Solution	SJ733 Mean FIC50	SJ733 FIC50 Standard Deviation	P218 Mean FIC50	P218 FIC50 Standard Deviation
1	1	0	0	0
2	0.97	0.21	0.26	0.11
3	0.98	0.20	0.66	0.13
4	0.65	0.13	0.97	0.052
5	0.24	0.062	0.94	0.080
6	0	0	1	0

Mean FIC50 values were calculated by averaging the three FIC50 values for each drug in each solution across data from the three plate sets. In other words, these are the results if one averaged the rows in Table 3. The standard deviations associated with these means are noted.

Discussion

The combined isobologram (Figure 11) combines data from all three sets of plates which were run (though as noted above, plates 2 and 3 were derived from the same input culture, so they are technically not biological replicates). The reference additive line displayed is the simplest way of analyzing drug-drug interactions with isobolograms, where data points above the line indicate antagonism and data points below the line indicate synergism. Since all data points on the combined isobologram lie above the reference line, this appears to indicate antagonism. However, true definitions of synergism and antagonism vary – two commonly used cutoffs are that the sum of the FIC's is below 0.5 for synergism, and above either 2 or 4 for antagonism²³. None of the summed FIC's for a given solution across any set of plates crosses the boundary of 2 for antagonism (though one comes close in plate set 3). Given the varying definitions of antagonism and the observation that this data doesn't meet one of the more common definitions of antagonism, we cannot conclusively say that SJ733 and P218 act antagonistically, just that they trend towards that direction. Opting to use software such as Calcsyn for this experiment may have incorporated more caveats and provided a clearer picture as to what interaction is occurring between SJ733 and P218. Other complications exist with the data, as discussed below in Future Directions.

An antagonistic interaction between SJ733 and P218 would not be expected given the independent mechanisms of action for these compounds – targeting PfATP4 for SJ733, and PfDHFR for P218. As described previously, the metabolic footprints of parasites treated by these two drugs also differ rather substantially, making it even less clear why an antagonistic interaction may be seen. One potential metabolic area of overlap for these two drugs is deoxyribonucleotides/nucleobases, as SJ733 caused a slight increase in some of these compounds while P218 caused a slight decrease in the same portion of the metaprint (see Figure 3, the furthest left hexagon in each drug's metaprint). The \log_2 fold changes in this area are very small, but potentially could present an area of conflict between the way the two drugs impact the parasite's metabolism, impacting each other's efficacy. If not metabolic, an interaction

between the drugs in terms of uptake may be another avenue to pursue (see here³⁵ for a brief mention of both compounds in terms of predicted drug absorption).

It is worth noting that, as described in the legend for Table 2, the IC₅₀ determination for many of the combinations tested across all plate sets suffered from statistical pitfalls (missing ends of 95% confidence intervals or completely lacking 95% confidence intervals) or in some cases, nonlinear regression fits which GraphPad designated “ambiguous.” GraphPad gives this property to nonlinear regressions in which at least one of the parameters has a best-fit value that is unreliable³⁶, even though the R² value may be good. These problems were likely due to suboptimal plate design – the assays had been intended to solidly delineate the top and bottom plateaus for each IC₅₀ curve, to ensure that the full range of action for each drug was captured. However, this led to very few data points on the curve between the two plateaus actually being recorded. This likely hampered curve fitting, leading to problematic regressions. Despite these issues, the data does appear to be rather consistent across the three sets of plates, lending reliability to the measurements.

A positive note is that the Atovaquone IC₅₀ value was rather consistent between the two individual drug plates, and the individual drug solutions (solutions 1 and 6) yielded IC₅₀ values that were close together across different sets of plates. These built-in controls help show that there likely was not much variance across experiments, as similar results were yielded for individual drugs between different plate setups.

The determined IC₅₀ values for SJ733 across the combination and individual experiments (37 nM +/- 4.1 nM, mean +/- standard deviation) fell very close to the published EC₅₀ value of 0.03 μM for 3D7 *P. falciparum*²⁹. The determined IC₅₀ values for P218 across the combination and individual experiments (0.41 nM +/- 0.037 nM, mean +/- standard deviation) were approximately 10-fold lower than the published value of 4.6 nM, though that experiment was performed on TM4 parasites using a [³H]-hypoxanthine incorporation assay³². The determined IC₅₀ values for Atovaquone (0.042 nM +/- 0.0022 nM, mean +/- standard deviation), only two data points from the individual drug experiments) were

approximately 25-fold lower than published values of approximately 1 nM for 3D7 parasites using SYBR Green assays^{37,38}.

Future Directions

There are many ways to evaluate dose-response curves and fixed-ratio drug combination results with isobolograms, and the simple method used in this study likely can be improved on. First, a linear additive reference line represents what one would expect given two drugs that have equal potencies and the same level of maximum killing. In other words, the individual IC_{50} curves for the two compounds being measured should be parallel and achieve the same lower-bound for parasite death. For such drugs, additivity is expected to present by the sum of the fractional IC_{50} 's totaling one at each ratio, indicating that the drugs do not interact with each other. In this set of experiments, I assumed the drugs achieved the same lower-bound for parasite death. Since both drugs are known to be good at clearing the parasite, this is probably an OK assumption. The larger underlying issue is that SJ733 and P218 appear to have rather different slopes for their dose-response curves. GraphPad evaluates the Hill Slope for nonlinear regressions such as those used here, which essentially describes how much steeper or shallower the curve is than a standard curve. In the individual drug assays, SJ733 was determined to have a Hill Slope of -9.533, while P218 had a Hill Slope of -3.057. This indicates that the two drugs have non-parallel dose-response curves, and as such the simple linear additive reference line may not be the best way to evaluate interactions. There are means of deriving curved isoboles for such pairs of drugs³⁹. However, it may be best to rerun the assays here with a larger emphasis on landing data points on the curve itself to improve curve fits before reanalyzing the data.

Another less technical means of verifying the data presented here would be to test pairs of known synergistic or antagonistic antimalarials. This would provide a point of reference to which the currently acquired data could be compared. I previously combined atovaquone and proguanil (known synergists) with a fixed-ratio plate design, but the results for proguanil did not make logical sense and as such the experiment was discarded. A number of synergistic and antagonistic pairs have been described in the literature, as compiled in this review²³, and so choosing representative pairs may not be such a difficult task.

When an antagonistic or synergistic combination is identified, it may be interesting to pursue study into where exactly the component drugs are interacting within the parasite's metabolism. One way to analyze this would be to extract metabolites from parasites given no drug, each drug individually, and the two drugs together. This project was not completed in favor of progressing to another area of research. However, this can be done with a methanol-based extraction for hydrophilic compounds, or an isopropanol-based extraction for lipids. The extracted metabolites can then be analyzed by liquid chromatography-mass spectrometry (LC-MS) for identification, and the relative amounts of metabolites can be compared between each experimental condition. By identifying metabolites that are significantly upregulated or downregulated between samples, we may be able to discern what pathways are impacted under the influence of individual drugs and how those pathways change when both drugs are combined.

Chapter 3

Discerning Metabolic Differences in *P. falciparum* Lipid Supplements

Introduction

In vitro culturing of *P. falciparum* requires a lipid supplement, as shown by only certain combinations of fatty acids (contained in reconstituted lipid-associated BSA) added to serum-free media supporting continuous culture⁴⁰. A follow-up study further narrowed down a specific lipid needed to optimize parasite growth⁴¹, and a chemically defined media was later produced which could sustain parasite growth⁴². While human serum (part of blood) is a logical choice and has long been used to fulfill this lipid requirement, there are valid concerns about its high cost and potentially unstable availability as well as the intrinsic variability that serum from different human donors will yield when used in experiments. A desirable alternative would be cheap and standardized to reduce costs and experimental variability. One such candidate to solve this problem is AlbuMAX (versions I and II are commercially available, differing in IgG content), which is widely used in labs such as ours and has been shown to be suitable as a culturing alternative in terms of growth rate, drug susceptibility, and transcriptional differences⁴³.

However, the literature is conflicting and impacts on parasite phenotypes have been documented when human serum vs. AlbuMAX or a mixture of both supplements is used. Infected erythrocytes grown in human serum have been found to bind certain endothelial receptors better than those grown in AlbuMAX, and the same study found significantly different gene expression (using next generation mRNA sequencing) in ring-stage FCR3 parasites grown in AlbuMAX vs. serum⁴⁴. The level of expression of PfEMP1, a family of important *P. falciparum* endothelial binding and antigenic variation proteins, has been shown to be significantly decreased in AlbuMAX-grown culture compared to serum-grown culture⁴⁵. Culture conditions have been shown to alter the duration of the asexual lifecycle, as parasites grown solely in AlbuMAX have a five-hour longer lifecycle than those grown in a

serum/AlbuMAX mixture (45 hours vs. 40 hours, respectively⁴⁶). Drug responses have even been shown to differ between AlbuMAX-only and serum/AlbuMAX cultures, specifically pyrimethamine and lumefantrine⁴⁶. Most interestingly, serum cultures produce more gametocytes than AlbuMAX cultures, and AlbuMAX media contains a reduced amount of multiple fatty acids compared to serum media⁴⁷. When AlbuMAX cultures were supplemented with fatty acids via phospholipids in vesicles, rates of gametocytogenesis could be recovered, indicating that fatty acids may play a key role in gametocytogenesis⁴⁷.

The last point addressed above is interesting because it is related to a seldom-discussed problem plaguing the field – AlbuMAX-grown asexual parasites can generate gametocytes, but they will not transmit to mosquitoes. This last point is something not published on (rather it is more of an accepted facet of the field), but it has long been known that serum is necessary for the best gametocyte maturation⁴⁸. It is for these reasons that transmission assays or studies otherwise looking at gametocytes typically use serum as the lipid supplement of choice⁴⁹⁻⁵¹ (this information is also based on personal communications with Michael Delves, Carole Long, and Kazutoyo Miura). Serum-grown asexual parasites have varying results, with “good” serum resulting in transmission and “bad” serum lacking it. This phenomenon leads to labs studying transmission having to rely solely on batches of “good” serum that they have found by chance from expensive, variable donor serum. Consequently, finding “good” serum is costly and unpredictable. Developing a cheaper, standardized alternative that could allow for the consistent generation of transmissible gametocytes is highly desirable, but AlbuMAX is clearly not yet that alternative due to the many phenotypic impacts described above. Understanding the metabolites present in “good” vs. “bad” serum as well as delving into how parasite metabolism changes upon transitioning parasites from AlbuMAX media to serum media (and vice-versa) may help pave the way for the development of an ideal transmission-oriented supplement. Research studying transmission deserves this important boost, as blocking parasite transmission is one important route of stopping disease spread and tackling the burden malaria imposes on humanity⁵².

Ongoing Efforts

To help understand what metabolites cause serum to be “good” vs. “bad” our lab is collaborating with the lab of Dr. Carole Long at the NIH. The Long lab has retained “good” and “bad” serum samples and conducted transmission experiments with treated serum – for example by using “good” serum that has been dialyzed, normal “good” serum that has been mixed with dialyzed “good” serum, or a reduced concentration of “good” serum. They then send aliquots of these sera to us for metabolomic analysis via LC-MS, where we attempt to find both hydrophilic and lipid compounds which are differentially present between “good” and “bad” serum. The answer so far does not seem to be one or two compounds alone that determine “goodness” for a certain serum sample – there are many compounds that differ between different types of serum (see Figure below). A talented postdoc who recently joined the lab is spearheading the analysis of all of the data we have on this project, hoping to uncover leads for future experiments to expand on.

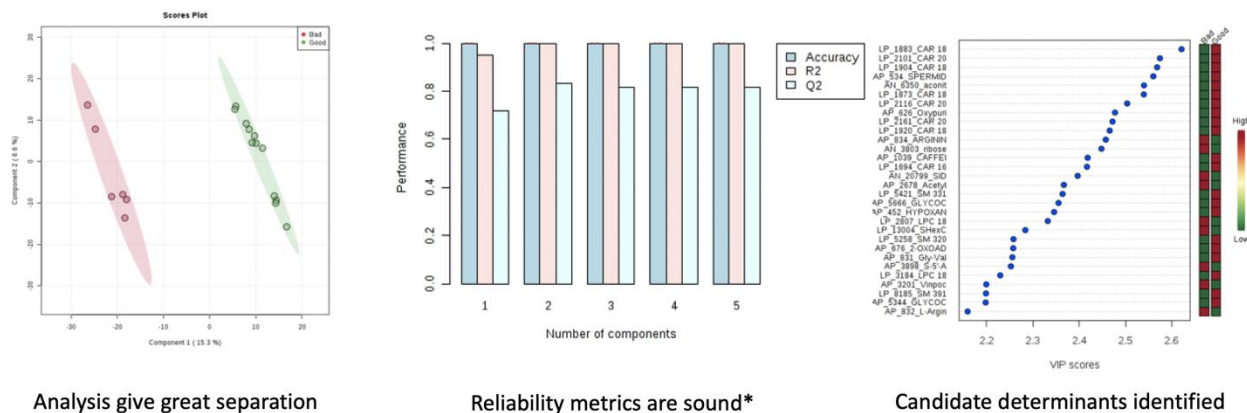


Figure 13: Good vs. Bad Serum Separation from One Sample Set

Serum samples from the first round of data collected by Erik Allman were analyzed by Gabe Rangel. The plot on the left is a PLS-DA demonstrating clear separation of good and bad serum based on metabolite data collected in aqueous positive, aqueous negative, and lipid positive modes. As depicted in the center, the data appears to be reliable. On the right, many compounds appeared to have comparably high VIP scores, indicating that there is no clear single compound that determines whether serum is good or bad – rather, many factors contribute. Many thanks to Gabe Rangel for this representation, done using MetaboAnalyst (see here for website⁵³).

Future Experimental Design

Experiments described in this section were curtailed by the COVID-19 pandemic. Given the numerous phenotypic changes that have been documented in the asexual parasite, we are also interested in evaluating how the metabolism of the parasite changes when a culture grown with one type of lipid supplement is switched over to the other (i.e. AlbuMAX → serum or vice-versa). Intriguingly, it has been anecdotally noted that switching from AlbuMAX to serum is relatively straightforward and does not alter the 48-hour asexual developmental cycle, while the opposite direction can cause a serious crash of the population, requiring a somewhat slow recovery. This further drives our interest in characterizing how the parasite responds to changing lipid supplements.

The AlbuMAX to serum transition makes for a good first step as the transition allows the parasite to continue growing well, which should facilitate relatively simple collection of enough parasites for metabolomic analysis. These experiments should focus on trophozoite metabolism, as this stage of the asexual life cycle is the most metabolically active. Our lab uses a magnetic separation protocol to isolate a highly pure population of trophozoites for metabolomic analysis – this procedure relies on the fact that trophozoites produce large hemozoin crystals which are magnetic, meaning that trophozoites can be selected for with the use of magnets.

We are not yet sure how long the parasites need to be in the “switched” media before metabolic changes will present. One possible route is to grow parasites in AlbuMAX as normal, perform a magnetic separation, and then transfer the separated trophozoites to serum media for two and a half hours prior to metabolite extraction, similar to drug mode-of-action tests which have previously been conducted in a similar manner²⁶. A parallel set of samples which are simply resuspended in AlbuMAX media (instead of switching to serum media) for 2.5 hours should be run as a control. Extracted metabolites can then be analyzed via LC-MS to compare metabolite levels between the switched serum samples and the control AlbuMAX samples to see what changes have occurred. This would provide a glimpse into metabolic changes that occur quickly after switching media types. For a more elongated exposure to the post-switch

media which may allow for slower changes to become apparent, it may be preferable to split a single flask of AlbuMAX-grown parasites into two parallel flasks, with one switched to serum media. This ensures that the original populations are identical and allows for continuation of the cultures in parallel for a number of days to let the switched parasites acclimate to the serum media. Then, the parallel cultures can be magnetically purified, and their metabolites extracted & analyzed via LC-MS.

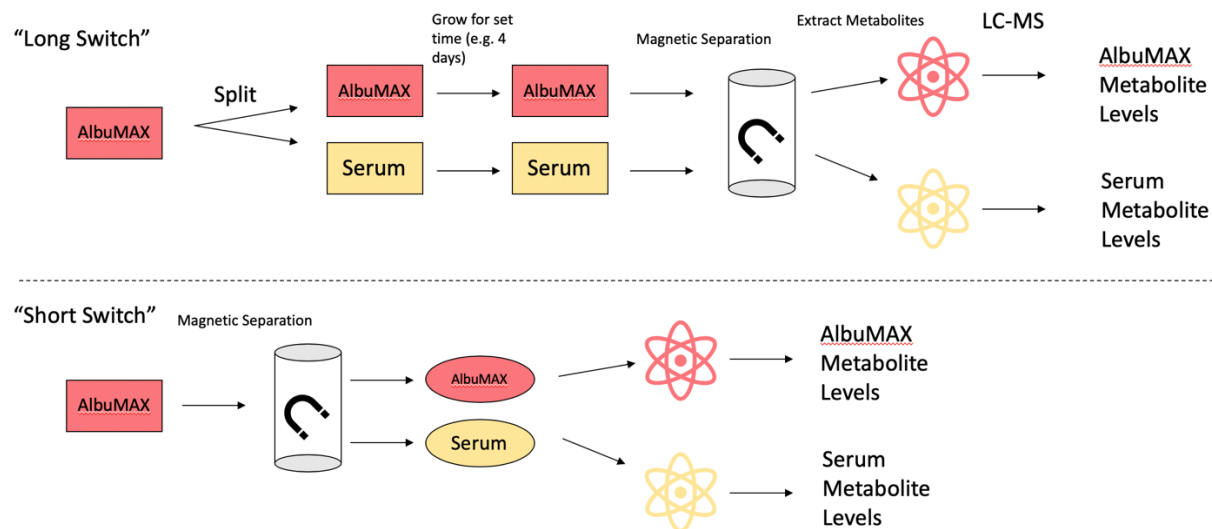


Figure 14: Sample AlbuMAX to Serum Transition Experiment Layouts

Pictured is a graphical representation of the above-described “short” and “long” AlbuMAX to serum transition experiments. As we do not know how long the parasite needs to adapt during this switch, it may be that both versions must be performed to determine optimal experimental conditions. The rectangular boxes and circles represent parasite cultures or magnetically separated suspensions, respectively, using the indicated lipid supplements.

The serum to AlbuMAX switch may yield more interesting results, as this is the “difficult” switch where populations of parasites have been known to crash post-switch. It is worth first attempting at least one of the aforementioned experimental designs to see if the population crash is reproducible, and if it is, to get an idea of whether or not there is still enough usable parasite material for magnetic purification and LC-MS analysis. If it turns out that the crash is too severe to switch media types immediately, a gradient switch should be considered. For example, if the starting media is 10% serum and the ending media is 0.5% AlbuMAX, an example gradient may be to use 10% serum, then 7.5% serum + 0.125% AlbuMAX, then 5% serum + 0.25% AlbuMAX, then 2.5% serum + 0.375% AlbuMAX, finishing at 0.5% AlbuMAX. The gradient can be made steeper or shallower depending on whether or not the parasites continue to crash during the switch. When parasites are able to be stably transitioned from serum media to AlbuMAX media, a similar protocol to the AlbuMAX to serum transition should be followed where a transitioned culture and parallel control (only ever grown in serum media) culture are grown, purified, and extracted alongside each other so that metabolite levels between the two conditions can be compared. If a gradient is able to be established in which the parasites are stable throughout the transition, it may be interesting to perform a sort of time-course experiment in which parasites are sampled throughout the transition for metabolomic analysis. This could provide an interesting view into the process by which the parasite changes its metabolism, as opposed to the other experimental designs which are more like endpoint comparisons.

Analysis of these datasets could first begin by looking only at metabolites which are on our knowns list – this will simplify the process and should skip the hassle of having to identify unknown compounds. However, the most interesting changes are not always in compounds that are reflected in our knowns lists, so it may be worth doing an untargeted analysis in the future to get a comprehensive view of how the entire parasite’s metabolism changes during these transition experiments. Additionally, one should consider whether they are interested in looking at both lipids and hydrophilic compounds, as we have no reason to believe that only one group or the other is impacted during transition. The two types of

compounds require different extraction procedures, so this should be carefully considered prior to the commencement of transition experiments.

It is hard to say what the expected results are for these experiments, but it would be reassuring if the results from one transition mirrored those from the other (that is, what is upregulated after transition from AlbuMAX to serum is downregulated in the opposite direction). If this does not happen, then something truly interesting may be at work where the parasite responds differently based on what supplement it begins in. Such experiments are sure to provide valuable insight into how different lipid supplements alter parasite metabolism, and hopefully can guide us towards the ideal supplement that the field has been looking for.

Appendix A

Commonly Used *P. falciparum* Culturing Protocols

Culture Maintenance

3D7 *Plasmodium falciparum* parasites were maintained in vented culture flasks (incubated at 37°C, 6% O₂, 5% CO₂, and 89% N₂) at 2% hematocrit in 0.25% Albumax in RPMI 1640 media. Culture medium was changed daily and parasitemia was monitored as needed by methanol fixation and Giemsa staining. Parasitemia was generally kept under 10% trophozoites, and cultures were split as required. When cultures were tested for mycoplasma, an e-Myco *plus* PCR Kit (Boca Scientific) was used.

Washing Blood

Male, O+ human blood was washed prior to *in vitro* use. Briefly, half of the desired final volume of blood was aliquoted into a 50 mL conical tube and resuspended to 50 mL total volume with 0.25% Albumax RPMI. The tube was mixed thoroughly and then centrifuged for 10 minutes at 2000-2300 RPM at 20°C. The supernatant was then aspirated. This wash was then repeated for a total of two washes, and the washed blood was resuspended with an equal volume of 0.25% Albumax RPMI to make a 50% blood in 0.25% Albumax RPMI mixture and was stored at 4°C for use *in vitro*.

Sorbitol Synchronization

To synchronize cultures which had become asynchronous with time (i.e. abundant ring and trophozoite stages at the same time), a sorbitol synchronization method was used as needed to eliminate trophozoites and select for rings. Briefly, a 5% sorbitol solution in water was pre-warmed to 37°C. The culture to be synchronized was transferred to a 50 mL conical tube and centrifuged at 1500 RPM for 5

minutes, followed by aspiration of the supernatant. The cell pellet was resuspended in 10x volumes of 5% sorbitol, mixed thoroughly, and incubated for 10 minutes in a 37°C water bath. The solution was then centrifuged at 1500 RPM for 5 minutes and the supernatant was aspirated. The cell pellet was resuspended in 10x volumes of 0.25% Albumax RPMI and centrifuged at 1500 RPM for 5 minutes, followed by aspiration of the supernatant. The cell pellet was then resuspended in the original volume of 0.25% Albumax RPMI and transferred to a fresh vented flask for incubation.

Culture Freezing

To freeze down stocks of *P. falciparum* parasites (ideally >5% rings), the entire culture volume was transferred to a 50 mL conical tube and centrifuged at 1500 RPM for 5 minutes at 20°C. The supernatant was aspirated and 0.3 volumes of Glycerolyte 57 solution was added to the cell pellet slowly and dropwise while gently shaking. The cells were then incubated at room temperature for 5 minutes before the slow, dropwise addition of 1.7 volumes of Glycerolyte 57. The cells were again incubated at room temperature for 5 minutes. Following incubation, approximately 1 mL of cells each were aliquoted to labeled cryovials and stored at -80°C.

Culture Thawing

To thaw frozen stocks of *P. falciparum* for culturing, a cryovial was thawed by hand and the contents were transferred to a 50 mL conical tube. 12% NaCl was added slowly and dropwise to a concentration of 100 µL per 1 mL of cells while gently shaking the tube, and the tube was then allowed to rest for 5 minutes at room temperature. 10x starting volumes of 1.6% NaCl was then added slowly and dropwise while gently shaking the tube, and the tube was immediately centrifuged at 1500 RPM for 5 minutes at 20°C. The supernatant was aspirated and 10x the starting volume of 0.9% NaCl +

2% glucose was added slowly and dropwise while gently shaking the tube. The tube was again centrifuged at 1500 RPM for 5 minutes at 20°C and the supernatant was aspirated. The cell pellet was resuspended in 10 mL of 0.25% Albumax RPMI at 2% hematocrit. The culture was transferred to a small vented culture flask and incubated at 37°C with 6% O₂, 5% CO₂, and 89% N₂.

Appendix B

Complete Normalized IC₅₀ Figures for Isobologram Construction

The following figures are the IC₅₀ curves from which the combination experiment FIC₅₀ values were derived. Note that since, as previously described, 0% was defined as the smallest value in each subcolumn and 100% growth was defined as the largest value in each subcolumn, the growth depicted here is relative. For all figures, “Sol” = solution. Data points represent averages from three technical replicate wells, and error bars represent the corresponding standard deviations.

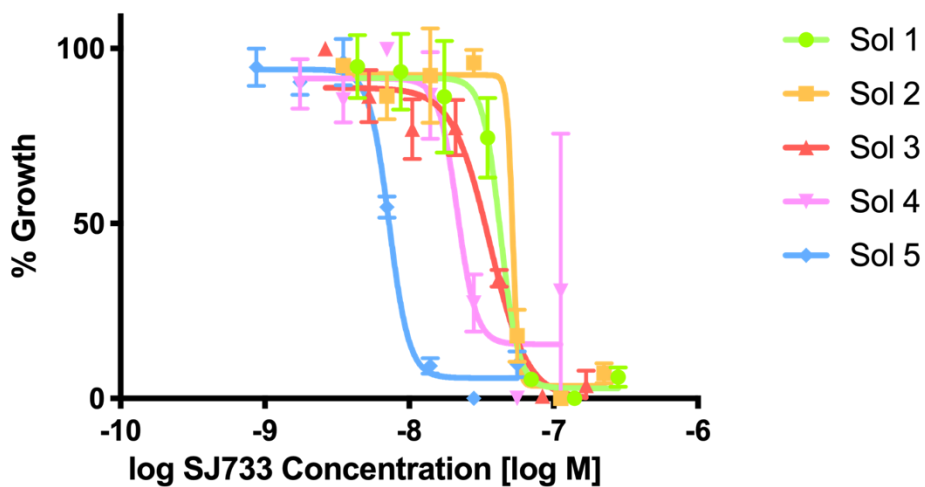


Figure 15: Normalized Relative Growth Data for SJ733 from Plate Set 1

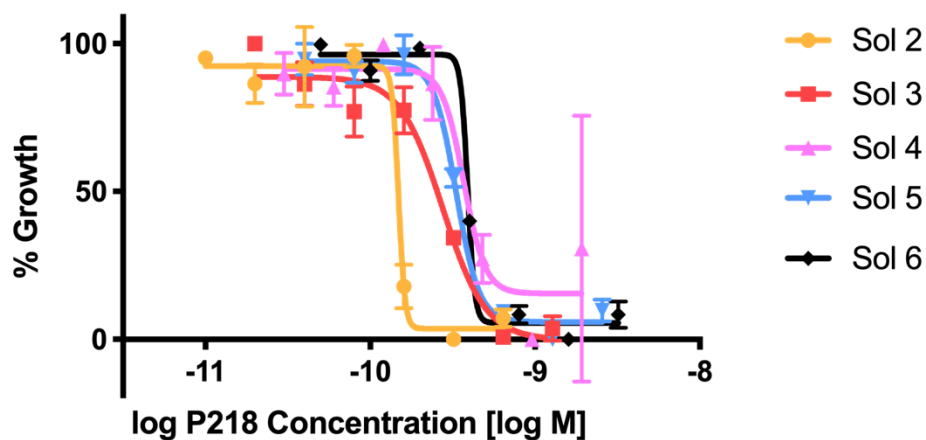


Figure 16: Normalized Relative Growth Data for P218 from Plate Set 1

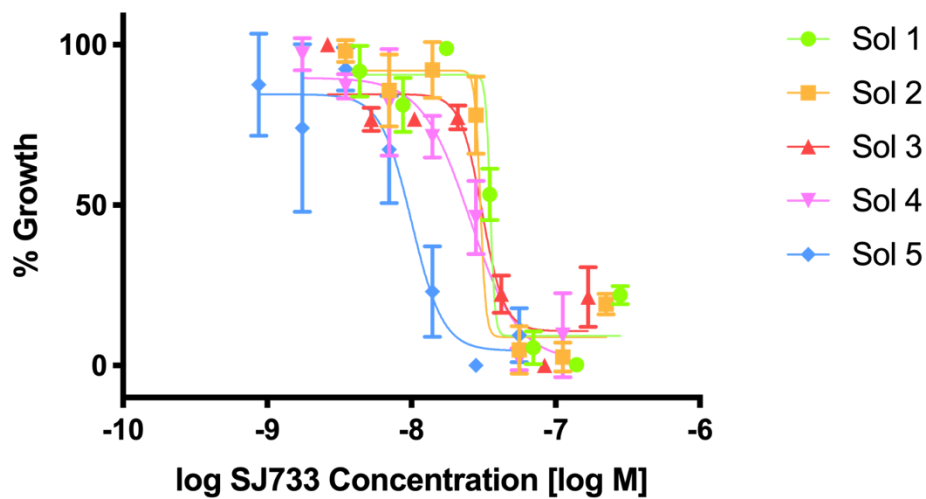


Figure 17: Normalized Relative Growth Data for SJ733 from Plate Set 2

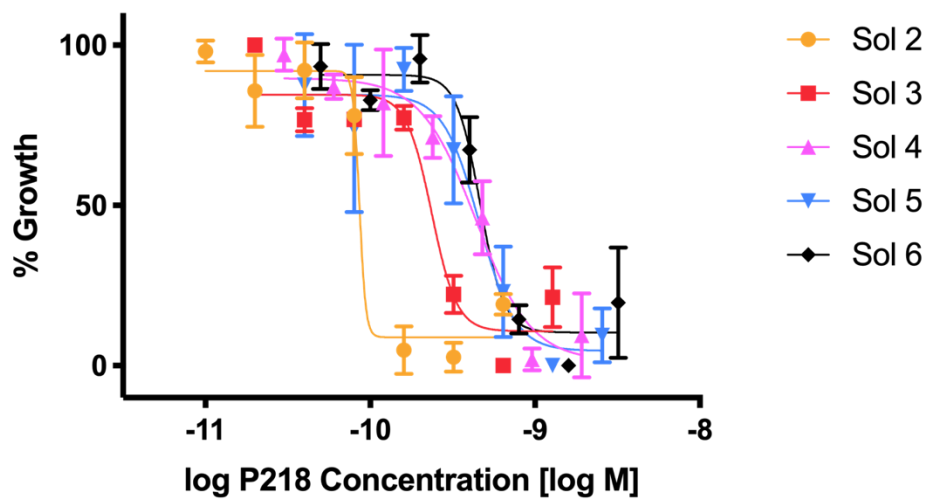


Figure 18: Normalized Relative Growth Data for P218 from Plate Set 2

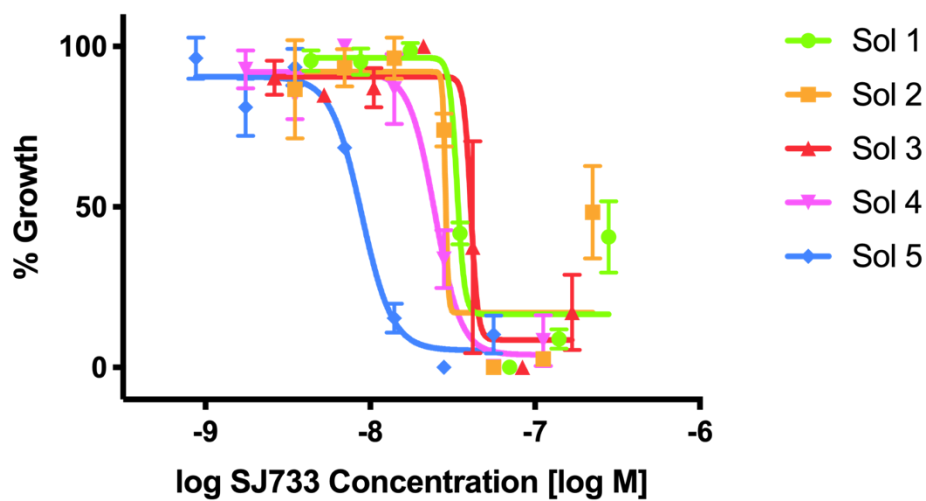


Figure 19: Normalized Relative Growth Data for SJ733 from Plate Set 3

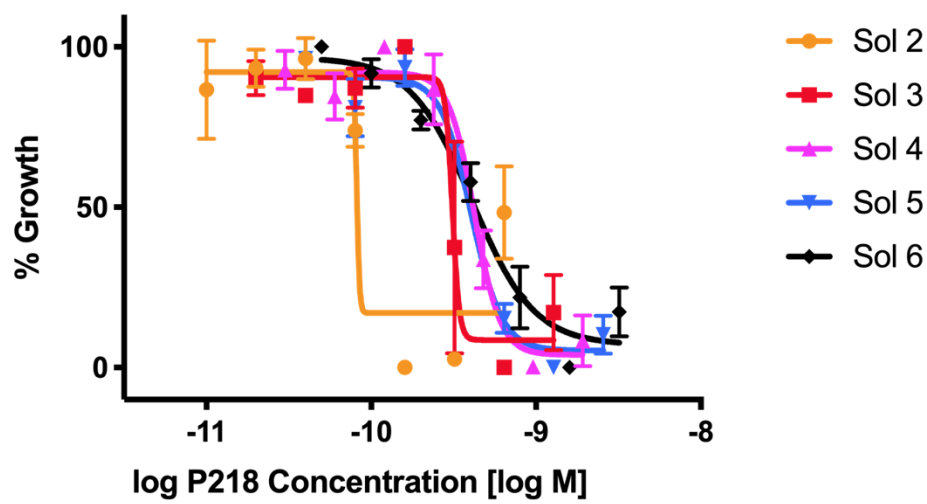


Figure 20: Normalized Relative Growth Data for P218 from Plate Set 3

BIBLIOGRAPHY

1. World Health Organization. *World Malaria Report 2019*. Geneva; 2019.
<https://www.who.int/publications-detail/world-malaria-report-2019>.
2. Rogerson SJ. Management of malaria in pregnancy. *Indian J Med Res*. 2017;146(September):328-333. doi:10.4103/ijmr.IJMR_1304_17
3. Cowman AF, Healer J, Marapana D, Marsh K. Malaria: Biology and Disease. *Cell*. 2016;167:610-624. doi:10.1016/j.cell.2016.07.055
4. Crutcher JM, Hoffman SL. Malaria. In: Baron S, ed. *Medical Microbiology*. 4th ed. Galveston (TX): University of Texas Medical Branch at Galveston; 1996.
<https://www.ncbi.nlm.nih.gov/books/NBK8584/>.
5. Miller LH, Ackerman HC, Su XZ, Wellems TE. Malaria biology and disease pathogenesis: Insights for new treatments. *Nat Med*. 2013;19(2):156-167. doi:10.1038/nm.3073
6. Dondorp AM, Lee SJ, Faiz MA, et al. The Relationship between Age and the Manifestations of and Mortality Associated with Severe Malaria. *Clin Infect Dis*. 2008;47(2):151-157.
doi:10.1086/589287
7. Tse EG, Korsik M, Todd MH. The past, present and future of anti-malarial medicines. *Malar J*. 2019;18:1-21. doi:10.1186/s12936-019-2724-z
8. World Health Organization. *World Health Organization Model List of Essential Medicines, 21st List, 2019*. Geneva; 2019. <https://apps.who.int/iris/bitstream/handle/10665/325771/WHO-MVP-EMP-IAU-2019.06-eng.pdf>. Accessed April 23, 2020.
9. White NJ. Antimalarial drug resistance. *J Clin Invest*. 2004;113(8):1084-1092.
doi:10.1172/JCI21682
10. Tilley L, Straimer J, Gnädig NF, Ralph SA, Fidock DA. Artemisinin Action and Resistance in

- Plasmodium falciparum. *Trends Parasitol.* 2016;32(9):682-696. doi:10.1016/j.pt.2016.05.010
11. Vaughan AM, Kappe SHI. Malaria parasite liver infection and exoerythrocytic biology. *Cold Spring Harb Perspect Med.* 2017;7(6):a025486. doi:10.1101/cshperspect.a025486
 12. Vaughan AM, Mikolajczak SA, Wilson EM, et al. Complete Plasmodium falciparum liver stage development in liver-chimeric mice. *J Clin Invest.* 2012;122(10):3618-3628. doi:10.1172/JCI62684
 13. Josling GA, Williamson KC, Llinás M. Regulation of Sexual Commitment and Gametocytogenesis in Malaria Parasites. *Annu Rev Microbiol.* 2018;72:501-519. doi:10.1146/annurev-micro-090817-062712
 14. Siciliano G, Alano P. Enlightening the malaria parasite life cycle: bioluminescent Plasmodium in fundamental and applied research. *Front Microbiol.* 2015;6:391. doi:10.3389/fmicb.2015.00391
 15. Rowe JA, Claessens A, Corrigan RA, Arman M. Adhesion of Plasmodium falciparum-infected erythrocytes to human cells: Molecular mechanisms and therapeutic implications. *Expert Rev Mol Med.* 2009;11:e16. doi:10.1017/S1462399409001082
 16. Chakraborty A. Understanding the biology of the Plasmodium falciparum apicoplast; an excellent target for antimalarial drug development. *Life Sci.* 2016;158:104-110. doi:10.1016/j.lfs.2016.06.030
 17. British Medical Journal. Treatment of pulmonary tuberculosis with streptomycin and para-aminosalicylic acid. *Br Med J.* 1950;2:1073-1085. doi:10.1136/bmj.2.4688.1073
 18. Frei E, Karon M, Levin RH, et al. The effectiveness of combinations of antileukemic agents in inducing and maintaining remission in children with acute leukemia. *Blood.* 1965;26(5):642-656. doi:10.1182/blood.v26.5.642.642
 19. White N. Antimalarial drug resistance and combination chemotherapy. *Philos Trans R Soc B Biol Sci.* 1999;354(1384):739-749. doi:10.1098/rstb.1999.0426
 20. Van Voorhis WC, Adams JH, Adelfio R, et al. Open Source Drug Discovery with the Malaria Box

- Compound Collection for Neglected Diseases and Beyond. *PLoS Pathog.* 2016;12(7):e1005763. doi:10.1371/journal.ppat.1005763
21. Medicines for Malaria Venture. MMV-supported projects. <https://www.mmv.org/research-development/mmv-supported-projects>. Published 2020. Accessed April 23, 2020.
 22. White NJ. Preventing antimalarial drug resistance through combinations. *Drug Resist Updat.* 1998;1(1):3-9. doi:10.1016/S1368-7646(98)80208-2
 23. Bell A. Antimalarial drug synergism and antagonism: Mechanistic and clinical significance. *FEMS Microbiol Lett.* 2005;253(2):171-184. doi:10.1016/j.femsle.2005.09.035
 24. Srivastava IK, Vaidya AB. A mechanism for the synergistic antimalarial action of atovaquone and proguanil. *Antimicrob Agents Chemother.* 1999;43(6):1334-1339. doi:10.1128/aac.43.6.1334
 25. Baggish AL, Hill DR. Antiparasitic agent atovaquone. *Antimicrob Agents Chemother.* 2002;46(5):1163-1173. doi:10.1128/AAC.46.5.1163-1173.2002
 26. Allman EL, Painter HJ, Samra J, Carrasquilla M, Llinás M. Metabolomic Profiling of the Malaria Box Reveals Antimalarial Target Pathways. *Antimicrob Agents Chemother.* 2016;60(11):6635-6649. doi:10.1128/AAC.01224-16
 27. Mott BT, Eastman RT, Guha R, et al. High-throughput matrix screening identifies synergistic and antagonistic antimalarial drug combinations. *Sci Rep.* 2015;5:13891. doi:10.1038/srep13891
 28. Matthews H, Deakin J, Rajab M, Idris-Usman M, Nirmalan NJ. Investigating antimalarial drug interactions of emetine dihydrochloride hydrate using CalcuSyn-based interactivity calculations. Bogyo M, ed. *PLoS One.* 2017;12(3):e0173303. doi:10.1371/journal.pone.0173303
 29. Jiménez-Díaz MB, Ebert D, Salinas Y, et al. (+)-SJ733, a clinical candidate for malaria that acts through ATP4 to induce rapid host-mediated clearance of Plasmodium. *Proc Natl Acad Sci U S A.* 2014;111(50):E5455-E5462. doi:10.1073/pnas.1414221111
 30. Gaur AH, McCarthy JS, Panetta JC, et al. Safety, tolerability, pharmacokinetics, and antimalarial efficacy of a novel Plasmodium falciparum ATP4 inhibitor SJ733: a first-in-human and induced

- blood-stage malaria phase 1a/b trial. *Lancet Infect Dis*. 2020. doi:10.1016/S1473-3099(19)30611-5
31. Ashley EA, Phyo AP. Plasmodium falciparum ATP4 inhibitors to treat malaria: worthy successors to artemisinin? *Lancet Infect Dis*. 2020. doi:10.1016/S1473-3099(20)30139-0
 32. Yuthavong Y, Tarnchompoo B, Vilaivan T, et al. Malarial dihydrofolate reductase as a paradigm for drug development against a resistance-compromised target. *Proc Natl Acad Sci U S A*. 2012;109(42):16823-16828. doi:10.1073/pnas.1204556109
 33. Fivelman QL, Adagu IS, Warhurst DC. Modified Fixed-Ratio Isobologram Method for Studying In Vitro Interactions between Atovaquone and Proguanil or Dihydroartemisinin against Drug-Resistant Strains of Plasmodium falciparum. *Antimicrob Agents Chemother*. 2004;48(11):4097-4102. doi:10.1128/AAC.48.11.4097-4102.2004
 34. GraphPad Software. Home - GraphPad. <https://www.graphpad.com/>. Accessed April 30, 2020.
 35. Basore K, Cheng Y, Kushwaha AK, Nguyen ST, Desai SA. How do antimalarial drugs reach their intracellular targets? *Front Pharmacol*. 2015;6:91. doi:10.3389/fphar.2015.00091
 36. GraphPad Software. GraphPad Prism 8 Curve Fitting Guide - "Ambiguous." https://www.graphpad.com/guides/prism/8/curve-fitting/reg_analysischeck_nonlin_ambiguous.htm. Accessed April 24, 2020.
 37. Agarwal P, Anvikar AR, Pillai CR, Srivastava K. In vitro susceptibility of indian plasmodium falciparum isolates to different antimalarial drugs & antibiotics. *Indian J Med Res*. 2017;146(5):622-628. doi:10.4103/ijmr.IJMR_1688_15
 38. Fisher N, Majid RA, Antoine T, et al. Cytochrome b mutation Y268S conferring atovaquone resistance phenotype in malaria parasite results in reduced parasite bc 1 catalytic turnover and protein expression. *J Biol Chem*. 2012;287:9731-9741. doi:10.1074/jbc.M111.324319
 39. Grabovsky Y, Tallarida RJ. Isobolographic analysis for combinations of a full and partial agonist: Curved isoboles. *J Pharmacol Exp Ther*. 2004;310(3):981-986. doi:10.1124/jpet.104.067264
 40. Mi-Ichi F, Kita K, Mitamura T. Intraerythrocytic Plasmodium falciparum utilize a broad range of

- serum-derived fatty acids with limited modification for their growth. *Parasitology*. 2006;133:399-410. doi:10.1017/S0031182006000540
41. Mi-Ichi F, Kano S, Mitamura T. Oleic acid is indispensable for intraerythrocytic proliferation of *Plasmodium falciparum*. *Parasitology*. 2007;134:1671-1677. doi:10.1017/S0031182007003137
 42. Asahi H. *Plasmodium falciparum*: Chemically defined medium for continuous intraerythrocytic growth using lipids and recombinant albumin. *Exp Parasitol*. 2009;121(1):22-28. doi:10.1016/j.exppara.2008.09.009
 43. Singh K, Agarwal A, Khan SI, Walker LA, Tekwani BL. Growth, drug susceptibility, and gene expression profiling of *Plasmodium falciparum* cultured in medium supplemented with human serum or lipid-rich bovine serum albumin. *J Biomol Screen*. 2007;12(8):1109-1114. doi:10.1177/1087057107310638
 44. Tilly AK, Thiede J, Metwally N, et al. Type of in vitro cultivation influences cytoadhesion, knob structure, protein localization and transcriptome profile of *Plasmodium falciparum*. *Sci Rep*. 2015;5:16766. doi:10.1038/srep16766
 45. Ribacke U, Moll K, Albrecht L, et al. Improved In Vitro Culture of *Plasmodium falciparum* Permits Establishment of Clinical Isolates with Preserved Multiplication, Invasion and Rosetting Phenotypes. Spielmann T, ed. *PLoS One*. 2013;8(7):e69781. doi:10.1371/journal.pone.0069781
 46. Duffy S, Avery VM. *Plasmodium falciparum* in vitro continuous culture conditions: A comparison of parasite susceptibility and tolerance to anti-malarial drugs throughout the asexual intraerythrocytic life cycle. *Int J Parasitol Drugs Drug Resist*. 2017;7(3):295-302. doi:10.1016/j.ijpddr.2017.07.001
 47. Tanaka TQ, Tokuoka SM, Nakatani D, et al. Polyunsaturated fatty acids promote *Plasmodium falciparum* gametocytogenesis. *Biol Open*. 2019;8(7):bio042259. doi:10.1242/bio.042259
 48. Lingnau A, Margos G, Maier WA, Seitz HM. The effects of hormones on the gametocytogenesis of *Plasmodium falciparum* in vitro. *Appl Parasitol*. 1993;34:153-160.

49. Miura K, Deng B, Tullo G, et al. Qualification of Standard Membrane-Feeding Assay with *Plasmodium falciparum* Malaria and Potential Improvements for Future Assays. *PLoS One*. 2013;8(3):e57909. doi:10.1371/journal.pone.0057909
50. Bolscher JM, Koolen KMJ, Van Gemert GJ, et al. A combination of new screening assays for prioritization of transmission-blocking antimalarials reveals distinct dynamics of marketed and experimental drugs. *J Antimicrob Chemother*. 2015;70:1357-1366. doi:10.1093/jac/dkv003
51. Delves MJ, Straschil U, Ruecker A, et al. Routine in vitro culture of *P. Falciparum* gametocytes to evaluate novel transmission-blocking interventions. *Nat Protoc*. 2016;11(9):1668-1680. doi:10.1038/nprot.2016.096
52. Burrows JN, Burlot E, Campo B, et al. Antimalarial drug discovery - The path towards eradication. *Parasitology*. 2014;141(1):128-139. doi:10.1017/S0031182013000826
53. Xia Lab at McGill University. MetaboAnalyst. <https://www.metaboanalyst.ca/>. Accessed April 30, 2020.

ACADEMIC VITA

Cuyler H. Luck

Education

The Pennsylvania State University, University Park, PA Class of May 2020
The Eberly College of Science | Bachelor of Science in Microbiology
The Schreyer Honors College | The Millennium Scholars Program

State College Area High School, State College, PA Class of June 2016

Experience

Undergraduate Research Assistant **University Park, PA**
The Pennsylvania State University, Dr. Manuel Llinás *September 2016-May 2020*

- Leverage **SYBR Green IC-50 assays** to evaluate drug interaction within antimalarial combination therapies
- Use **LC-MS** to uncover metabolic differences in samples of, or parasites cultured in, artificial or human-derived culture lipid supplements that may impact *Plasmodium falciparum* gametocyte transmissibility
- Perform metabolomic data analyses, visualization, and database construction using **R**

Summer Research Intern — U. Penn Summer Undergraduate Internship Program **Philadelphia, PA**
The University of Pennsylvania, Dr. Lewis Chodosh *June 2018 - August 2018, June 2019 - August 2019*

- **2018:** Employed **droplet digital PCR** to quantify the absolute number of tumor cells in a **doxycycline-inducible Her2/neu mouse model of breast cancer dormancy**
- **2019:** Expanded on 2018 studies to evaluate the suitability of droplet digital PCR for competition assays aimed at identifying genes important for tumor dormancy
- Prepared and imaged **immunofluorescence slides** for breast cancer dormancy assays

Summer Research Intern — MD Anderson Summer Program in Cancer Research **Smithville, TX**
The University of Texas MD Anderson Cancer Center, Dr. Blaine Bartholomew *June 2017 - August 2017*

- Performed **large-scale protein purification** of SWI/SNF chromatin remodeler from mutant *S. cerevisiae* strains
- Characterized cancer-associated mutations in SWI/SNF using nucleosome binding and remodeling assays
- Constructed epitope-tagged *S. cerevisiae* strains via **transformation** and verified results using **growth assays** and **sequence verification**

Research Assistant **University Park, PA**
The Pennsylvania State University, Dr. Jonathan Trump *June 2014-October 2015*

- Studied Active Galactic Nuclei and their characteristics at various redshifts
- Programmed with IDL to create diagrams analyzing thousands of catalogued galaxies
- **Contributed to published research paper** and extended on work to write **competitive research paper** for submission to the Siemens Competition in Math, Science, and Technology

Publications

1. Trump, J. R., Sun, M., Zeimann, G. R., **Luck, C.**, Bridge, J. S., Grier, C. J., ... and Brandt, W. N. (2015). The Biases of Optical Line-Ratio Selection for Active Galactic Nuclei and the Intrinsic Relationship between Black Hole Accretion and Galaxy Star Formation. *The Astrophysical Journal*, 811(1), 26.

Oral Presentations

1. **Luck C**, Sreekumar A, Marino F, Egunsola A, and Chodosh L. *A Novel Method to Quantify Minimal Residual Disease in Breast Cancer Dormancy*. Leadership Alliance National Symposium, Hartford, CT. July 27, 2019.
2. **Luck C**, Marino F, Kim J, Sreekumar A, Belka G, and Chodosh L. *Quantifying Minimal Residual Disease in Breast Cancer Dormancy*.
 - A. Annual Biomedical Research Conference for Minority Students, Indianapolis, IN. November 17, 2018.
 - B. Leadership Alliance National Symposium, Hartford, CT. July 28, 2018.

3. **Luck C** and Zhang S. *Screening human cancer-associated mutations of the SWI/SNF chromatin remodeler in yeast*. Summer Program in Cancer Research Student Symposium, Smithville, TX. August 11, 2017.
4. **Luck C** and Zhang S. *Constructing epitope-tagged mutations in the yeast SWI/SNF chromatin remodeler for whole-genome ChIP-seq*. Summer Program in Cancer Research Student Symposium, Smithville, TX. August 11, 2017.

Poster Presentations

1. **Luck C**, Sreekumar A, Marino F, Egunsola A, and Chodosh L. *A Novel Method to Quantify Minimal Residual Disease in Breast Cancer Dormancy*. Summer Undergraduate Internship Program Research Symposium, Philadelphia, PA. August 8, 2019.
2. **Luck CH**, Allman E, Llinás M. *Searching for interactions between treatments against *P. falciparum**. Penn State Undergraduate Research Exhibition, University Park, PA. April 17, 2019.
3. **Luck C**, Marino F, Kim J, Sreekumar A, Belka G, Egunsola A, and Chodosh L. *Quantifying Minimal Residual Disease in Breast Cancer Dormancy*.
 - A. Eberly College of Science Poster Exhibition, University Park, PA. September 25, 2018.
 - B. Summer Undergraduate Internship Program Research Symposium, Philadelphia, PA. August 9, 2018.
4. **Luck C**, Zhang S, Persinger J, Kundu S, Hailu SG, and Bartholomew B. *Screening human cancer-associated mutations of the SWI/SNF chromatin remodeler in yeast*.
 - A. Penn State Undergraduate Research Exhibition, University Park, PA. April 18, 2018.
 - B. Penn State Student Engagement Exposition, University Park, PA. November 6, 2017.
 - C. Penn State Eberly College of Science Benefactor Recognition Dinner, University Park, PA. October 5, 2017.

Skills

- Cell culture (*P. falciparum*, *S. cerevisiae*, human)
- Gel electrophoresis (agarose, SDS-PAGE)
- PCR (standard, droplet digital)
- Immunofluorescence staining and imaging
- Intermediate level of programming in **R**
- Basic level of programming in **Python** and **Java**
- Intermediate usage of **Microsoft Office**
- Intermediate usage of **Adobe Premiere Pro** and **Lightroom**
- Basic **French**

Memberships

League Club at Penn State

The Pennsylvania State University

University Park, PA
January 2019-May 2020

- Content Chair, 2019-2020 Academic Year
- Coordinate shoutcasters and manage club Twitch.tv channel to broadcast club activities
- Oversee and help produce content for club YouTube channel
- Academy Player, Spring of 2018-2019 Academic Year
- Play in intercollegiate and amateur League of Legends tournaments

Cohort Council, Millennium Scholars Program

The Pennsylvania State University

University Park, PA
June 2018-May 2020

- Meet with program administrators to discuss student and program needs
- Elected by peers to co-represent a cohort of Scholars

Science LionPride

The Pennsylvania State University

University Park, PA
September 2016-December 2019

- Serve as an ambassador for the Eberly College of Science at service and alumni events
- Give tours for prospective students (21 tours) and aid at outreach events

Penn State Speech & Debate Society

The Pennsylvania State University

University Park, PA
December 2016-May 2019

- Vice President, 2018-2019 Academic Year
- Oversaw and participated in public debates and outreach events
- Produced model debate for local elementary school learning enrichment programs — *Feb. 2019*
- Coordinated visit from British students for a public debate — *Oct. 2018*

- Facilitated forum on Citizens and Police Misconduct — *Apr. 2018*
- Advised local elementary school students on oral argumentation skills — *Jan. 2018*
- Filmed model debate for a Penn State World Campus course — *Dec. 2017*
- Debated in MLK, Jr. Commemoration Debate — *Jan. 2017*
- Sixth Place Speaker in NFA-LD Debate, 2017 Lafayette OCHOIE Tournament
- Second Place Speaker in NPDA Debate, 2017 PA Forensics Association State Tournament

American Society for Microbiology, Penn State Chapter

The Pennsylvania State University

University Park, PA

August 2016-May 2017

- Discussed research conducted by Microbiology undergraduates and faculty members at PSU

Teaching and Mentorship

Learning Assistant

The Pennsylvania State University

University Park, PA

August 2018-May 2020

- **BIOL 222**, Genetics (2 times): Attend lectures and hold weekly problem-solving sessions to help students understand genetics concepts. **Lead LA** in Fall 2019: Additionally coordinate two student LA's in their roles.
- **BIOL 322**, Genetic Analysis (2 times): Hold weekly problem-solving sessions to guide students through homework, quiz, exam, and lecture material. **Lead LA** in Spring 2020: Coordinate five student LA's.

Peer Mentor

The Pennsylvania State University

University Park, PA

August 2018-May 2020

- Mentor and advise four Millennium Scholar underclassmen throughout the academic year on topics such as getting into a research lab and finding summer research internships

Learning Assistant Facilitator

The Pennsylvania State University — Center for Excellence in Science Education

University Park, PA

May 2019

- Aided with workshops on evidence-based teaching strategies for ~40 Penn State Eberly College of Science faculty

High School Debate Coach

State College Area High School

State College, PA

September 2016-December 2018

- Teach a group of more than 15 high school students how to construct and deliver arguments
- Supervise practices and accompany team to regional tournaments

Undergraduate Tutor

The Pennsylvania State University

University Park, PA

September 2017-December 2018

- Tutor undergraduate students in introductory biology and microbiology courses

Academic Honors

Schreyer Academic Excellence Scholarship

August 2016 – May 2020

Millennium Scholars Program Scholarship

June 2016 – May 2020

Eberly College of Science Spring 2020 Commencement Marshal

May 2020

John Sr. and Kimlyn Patishnock Grand Prize — PSU Undergraduate Research Exhibition

April 2019

Best Insight — Penn State DataFest 2019

April 2019

Eberly College of Science Undergraduate Research Support Awardee

November 2018

Outstanding Oral Presentation — ABRCMS 2018

November 2018

Schreyer Honors College Travel Grant

November 2018

Daniel R. Terzhak Memorial Scholarship in Molecular and Cell Biology

September 2018

PSU Speech & Debate Society Excellence in Public Engagement Award

April 2018

Best Overall Presentation and Best Insight — Penn State DataFest 2018

April 2018

Evan Pugh Scholar Senior Award

March 2018

Phi Kappa Phi Society

January 2018

National AP Scholar

August 2016

National Merit Scholar

March 2016

Presidential Scholar Candidate

February 2016